MSc Biomedical Engineering
Final Project

Assessing changes in EEG functional connectivity after dual-site transcranial Alternating Current Stimulation for varied phase lags

Brighton de Jong

Supervisor: Dr.ir. Bettina Schwab (chair of the committee)
Daily supervisor: ir. Silvana Huertas Penen
External member: Dr.rer.nat. Maria Carla Piastra

June, 2024

Department of Biomedical Signals and Systems
Faculty of Electrical Engineering,
Mathematics and Computer Science,
University of Twente

UNIVERSITY OF TWENTE.

Contents

Abstract

Background: Functional connectivity (FC) is known to be altered in various neurological disorders. Dual-site transcranial Alternating Current Stimulation (tACS) is hypothesized to modulate FC, potentially improving motor-related symptoms when targeted at the primary motor cortex (M1). Our main objective was to investigate the phase lag condition because it is a fundamental parameter in dual-site tACS to modulate FC. However, the specific effects of the phase lag remain poorly understood, as there is high variability in results. In addition, only in-phase and anti-phase conditions have been previously investigated. Furthermore, the optimal method for measuring FC and the appropriate dual-site tACS parameter settings remain ambiguous. Therefore, our secondary objective is to systematically analyze FC measures and parameter settings to recommend the most effective configurations for future research.
Methods: In this study, we have measured resting-state EEG to investigate the impact of dual-site tACS on the beta-band FC between bilateral M1s by examining four phase lag conditions and a sham condition for nine healthy young participants (aged 18-34 years). The four phase lags were used: 0 (in-phase, IP), $\pi/2$ (pi-half, PH), π (anti-phase, AP), and $3\pi/2$ (three-half-pi, 3HP). Circular statistics, using the Mean Vector Length (MVL) in conjunction with permutation statistics, were employed to assess uniformity across the phase lags while averaging the observed change in FC across all participants for each phase lag condition. Subsequently, multiple comparisons tests, including Bonferroni-correction, were conducted between all five conditions. The statistical tests were performed for ImCoh and wPLI, across four parameter settings: electrode pair selection, frequency band, epoch length, and averaging type.
Results: For an average over three electrode pairs (FCC3h-FCC4h, C5-C6, and FC5-FC6), a beta-band frequency range of 13-30 Hz, an epoch length of 20s, using averaging type 1, we observe a significant non-uniform distribution across the four phase lags. This was found for wPLI ($p=0.017$), but not for ImCoh ($p=0.187$). Subsequent multiple comparisons tests revealed a significant difference between SH-AP ($p=0.039$) and IP-AP ($p=0.022$). These differences were due to a relative increase in FC for AP.
Conclusions: Our dual-site tACS study, which investigated four types of phase lags, has revealed the uncommon finding of increased FC for AP compared to IP and SH. This result underscores the variability in phase lag outcomes in dual-site tACS, highlighting the need for further investigation. As we found significant results for wPLI where ImCoh did not, we suggest using wPLI over ImCoh as the FC measure. Additionally, we identified a different electrode pair group for capturing changes in FC than initially expected. Further investigation in our ongoing study, incorporating spatial filtering, source reconstruction, and a larger sample size, is warranted to enhance the statistical power and reliability of these findings.

Keywords: non-invasive brain stimulation, dual-site transcranial Alternating Current Stimulation, phase lag, functional connectivity, imaginary coherence, weighted Phase Lag Index, beta-band, primary motor cortex, electroencephalogram

1 Introduction

1.1 Transcranial alternating current stimulation

Abnormal brain wave patterns have been observed in various neurological and psychiatric disorders, such as such as Parkinson's Disease [1], Alzheimer's Disease [2], depression [3] and Schizophrenia [4]. There is growing interest in the development of methods to externally modulate these neural oscillations to potentially alleviate symptoms of these patients [5]. Transcranial alternating current stimulation (tACS) is a non-invasive brain stimulation technique utilized to modulate brain oscillations and potentially improve motor- and cognitive-related functions [5–8]. By delivering weak alternating currents through electrodes placed on the scalp, tACS generates an electric field that targets the outer layers of the brain, specifically the cortical areas [5]. In traditional tACS, only a single electrode provided the alternating current [7, 9–11]. High-definition (HD) tACS tends to be more commonly used [12–16] and considered to be more accurate in targeting the region of interest [16]. HD-tACS stems from the field of transcranial Direct Current Stimulation (tDCS) [17–19]. It was initially developed for tDCS and later translated to tACS in 2014 [15, 20]. For HD-tACS, a center electrode produces a weak alternating current [7] ranging from 1 to 4 mA peak-to-peak [21]. To comply with Kirchhof's circuit rule [5], the outer electrodes collectively generate a counteractive current of equal magnitude to that of the center electrode, ensuring a net zero current flow.

Figure 1 [5] illustrates an example wherein the red electrode represents the center electrode and the blue electrodes represent the outer electrodes with an opposite current. Each electrode carries one-fourth of the current of the central electrode. The electric field produced is expressed as millivolts per millimeter (mV/mm) and is generally in the range of 0.1 to 1 mV/mm [5].

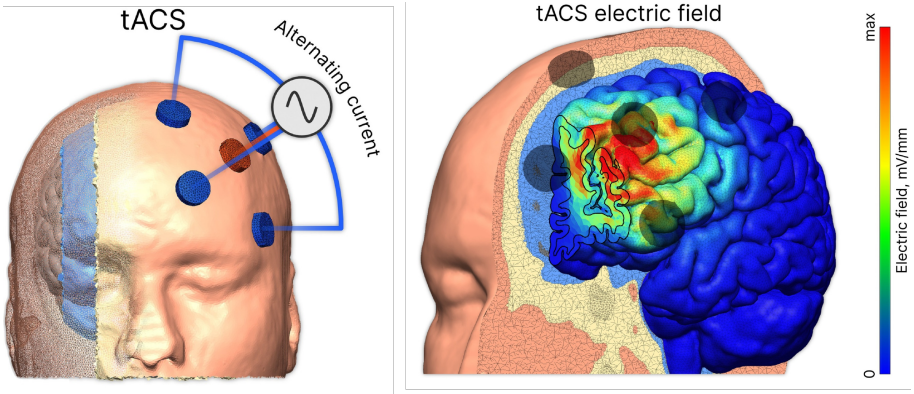

FIGURE 1: 4 to 1 tACS electrode montage. On the left, the center electrode (red) and the outer electrodes (blue) are demonstrated. On the right, is an example illustrating how the electric field is concentrated around the position of the red electrode. Figure is taken from Wischnewski et al. (2023) [5].

The working hypothesis is that entrainment is the main underlying mechanism of tACS [5, 22, 23]. Entrainment occurs when (some) brain oscillations synchronize with the frequency of the external alternating current applied [5]. Figure 2 [5] illustrates this phenomenon. The grey dots represent the pre-stimulation state, where neuronal spiking is relatively disorganized. Subsequently, when the alternating current is applied, it generates an electric field that influences the timing of the spiking of the neurons, as depicted by the pink dots. That is, neurons align with the frequency of the alternating current. This can be described as the temporal locking of brain oscillations with the given electrical stimulus [5].

While not all neurons synchronize with the given frequency stimulus, as observed in studies examining the effects of tACS in nonhuman primates [22, 23], the synchronized activity of some neurons could be sufficient to alter the brain state. This effect has the potential to enhance cognitive and motor functions, depending on factors such as the site of application, frequency, and dosage of the stimulation [5, 21].

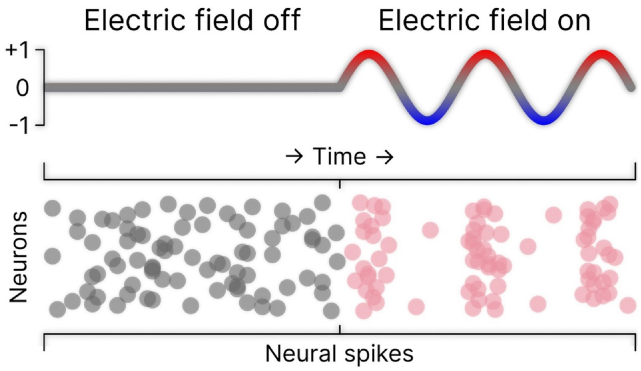

FIGURE 2: Entrainment - the effect of tACS when turning the stimulation on. The black dots represent neural spikes before stimulation (disorganized) and the pink dots represent neural after stimulation (synchronized with the stimulation). Figure is taken from Wischnewski et al. (2023) [5].

Observed stimulation-outlasting effects of tACS are hypothesized to be caused by spike-timing-dependent plasticity (STDP) [24]. This theory assumes that tACS entrains a subset of the targeted neurons, leading to a form of synaptic plasticity reliant on the precise timing of action potentials between pre-synaptic and post-synaptic neurons [24, 25]. When a pre-synaptic action potential precedes a post-synaptic potential, long-term potentiation occurs, strengthening the synapse and increasing the likelihood of future pre-synaptic influence on post-synaptic activity. Conversely, if the post-synaptic potential precedes the pre-synaptic action potential, long-term depression occurs, weakening the synapse [25]. During tACS application, the (partial) entrainment of neuronal oscillations modulates the timing of spikes, leading to the strengthening or weakening of synapses, and thus creating lasting changes in brain connectivity and function.

1.2 Dual-site tACS

As mentioned before in 1.1, abnormal brain oscillations have been implicated in various neurological and psychiatric disorders (1.1). Abnormal brain waves affect not only individual brain regions but also communication between multiple regions [14, 26, 27]. Specifically, the functional connectivity (FC) between distant cortical areas plays a crucial role in facilitating the flow of information across the brain [5, 15]. Thus, researchers have explored the application of tACS simultaneously in more than one cortical area [9, 11, 12, 14–16, 28, 29]. In dual-site tACS, electrical stimulation is administered to two distinct cortical regions concurrently.

In particular, when dual-site tACS is applied with a frequency within the beta range (e.g. 20 Hz), it holds promise for modulating motor and cognitive function [12, 13, 30]. Specifically, this technique targets response inhibition [12, 13] and the regulation of current motor states [30]. When these control mechanisms malfunction, the ability to transition between different coordination patterns may be compromised.

1.3 Phase lag

One variable that comes inherently when applying tACS to two sites is the difference in phase between the two applied stimuli, also called the phase lag. When this phase lag is equal to zero, it is called in-phase stimulation. This means that the sinusoidals applied with tACS on both sites have the same peaks and troughs aligned over time, as well as their frequency and amplitude. Various phase lags can be introduced between the two stimulated regions. For example, anti-phase stimulation can be applied, characterized by a phase lag of π, where the peaks and troughs of the sinusoidal forms are exactly opposite to each other. Figure 3 includes a visualization of both in-phase and anti-phase stimulation, where dual-site tACS was applied on the left and right hemisphere [14]:

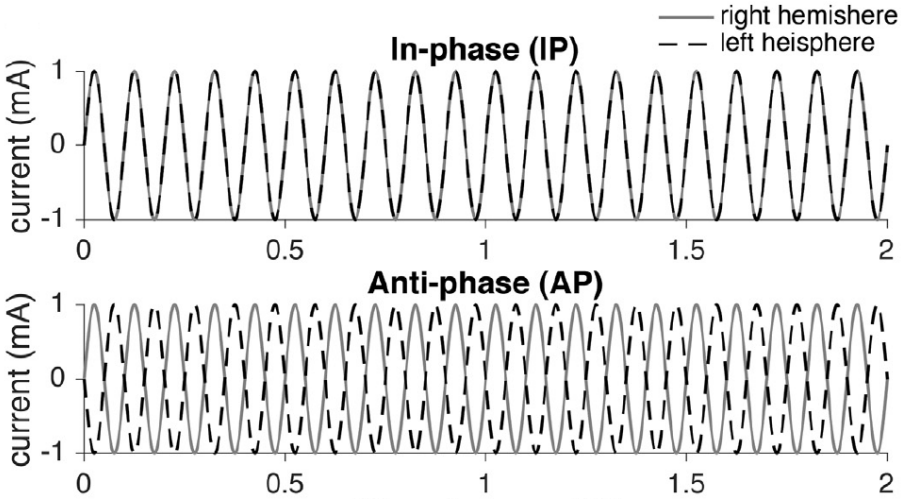

FIGURE 3: Example of in-phase and anti-phase stimulation in dual-site tACS, applied on the left and right hemispheres. Figure taken from Schwab et al. (2019) [14].

The effects of in- and anti-phase stimulations have been previously investigated [9–16, 28–30] for dual-site tACS. Generally, most studies report that in-phase and anti-phase stimulations exert different, or even opposing effects on the inter-regional communication between the targeted cortical areas ([9, 12, 14, 15]). However, not all studies show this in their results by reporting no change in FC ([13, 29]), or even reported that anti-phase showed increased FC while in-phase did not [10]. Additionally, the effects of other phase lags (e.g. π and $3\pi/2$) remain unexplored. This warrants further investigation to explore the effects of multiple phase lags in dual-site tACS.

1.4 Functional connectivity

FC refers to the statistical dependencies between time series of neuronal activation patterns across different regions of the brain [31]. This concept is pivotal in neuroscience for understanding how brain regions communicate and coordinate with each other. It is essentially a measure of how brain activity in different regions is synchronized over time [31]. It is important to note that FC is a statistical concept that does not directly infer causality, that is, the observed temporal correlation between brain regions does not necessarily mean that activity in one region causes activity in another [31].

Dual-site tACS holds promise for modulating the functional connectivity (FC) between cortical areas [16, 24, 32]. By targeting specific frequencies that are naturally present in the brain's oscillatory activity, dual-site tACS can potentially enhance or diminish the synchronization between cortical areas, thereby modulating the FC between them (reference).

FC plays a crucial role in brain function and has been implicated in a wide range of neurological disorders (references). Dual-site tACS allows for the simultaneous application of tACS to multiple cortical areas, offering the potential to modulate FC. A modulation could be beneficial in the clinical setting, depending on whether the patient has cortical areas exhibiting either excessive or deficient FC (references).

1.4.1 Base of FC measures: phase clustering

There are various approaches [10–15, 29, 33] to measure FC within the application of dual-site tACS. The measuring method of most of these FC measures is based on inter-site phase clustering (ISPC), which describes in which quantity the phase difference is consistent over time between the two sites (i.e. regions) of interest [34]. When the phase difference is consistent, it is correlated to a high level of FC.

This phase difference is often also referred to as the phase lag. In the context of dual-site tACS and FC, this can be confusing. The difference is that the phase lag in dual-site tACS is an input phase difference between the two given stimuli and the phase lag in FC is the measured output phase difference between two electroencephalogram (EEG) signals.

Another possible confusion is the word 'lag', as in the context of connectivity this can refer to that one signal lags the other i.e. the opposite of a phase lead. However, in FC analysis, the phase lag or lead is not considered. The term phase lag refers to the absolute phase difference between signals when measuring FC.

In an effort to avoid confusion, from now on, phase lag (without hyphen) is used to refer to the input phase difference in dual-site tACS. The term phase-lag (with hyphen) is used to refer to the measured phase-lag between EEG signals, in the context of quantifying FC.

Continuing with the investigation of a consistent phase-lag over time, we further elaborate on the calculation of ISPC. An example involving two EEG signals from electrodes x and y is provided. Both signals are sinusoidal and have an amplitude (m_x, m_y) and phase component (ϕ_x, ϕ_y) such that they can be described as $m_x * e^{i\phi_x}$ and $m_y * e^{i\phi_y}$. With a focus on the phase component, ISPC looks for whether the signals x and y are showing a constant phase difference $\Delta\phi$ over time. Within the example of signals x and y, we can subtract these signals from each other to obtain equation 1:

$$e^{i\phi_x} - e^{i\phi_y} = e^{i(\phi_x - \phi_y)} = e^{i\Delta\phi} \quad \text{with} \quad \Delta\phi = \phi_x - \phi_y \tag{1}$$

To then have a look at whether the phases of x and y are functionally connected, we must look at the phase angle difference. To obtain the phase angle difference, we first need to obtain the phase angles of both signal x and y over time. To perform this transformation, we can apply a Morlet Wavelet Convolution (MWC). It is a convolution of the narrowband (snippet from broadband) filtered signal with a complex Morlet wavelet [34]. MWC derives both a frequency component and a phase angle component and keeps the time component. After transformation, three features are extracted: amplitude, phase and narrowband filtered signal [35]. All these features can then be plotted over time. For the application in our example, we transform EEG signals x and y such that we extract their phase component and have a phase angle over time plot. This transformation is illustrated in Figure 4:

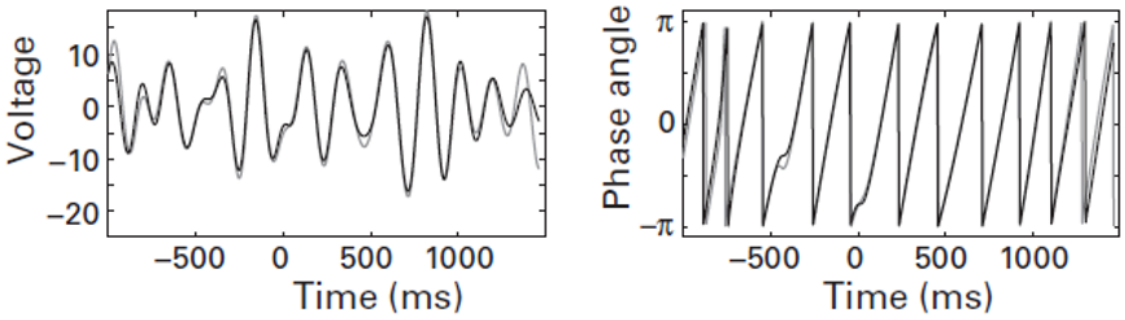

FIGURE 4: The figure on the left shows the original two exemplary EEG signals x and y. The figure on the right shows the same signals x and y after MWC, now displaying the phase angle over time of both these signals. Figures taken from Cohen (2014) [34].

Using Equation 1, with MWC we can also obtain this formula with a time component t (Equation 2).

$$e^{i\phi_{xt}} - e^{i\phi_{yt}} = e^{i(\phi_{xt} - \phi_{yt})} = e^{i\Delta\phi_t} \quad \text{with} \quad \Delta\phi_t = \phi_{xt} - \phi_{yt} \tag{2}$$

When applying Equation 2, we obtain the phase angle difference of signals x and y. The phase angle time series from Figure 4 is then converted to a phase angle difference time series in Figure 5a.

When projected onto the complex plane, we obtain Figure 5b. In this figure, each line represents a phase angle difference. After collecting these multiple phase differences across various time points, it can be evaluated whether these obtained phase differences consistently show a similar value. This would then indicate that both brain regions are functionally connected.

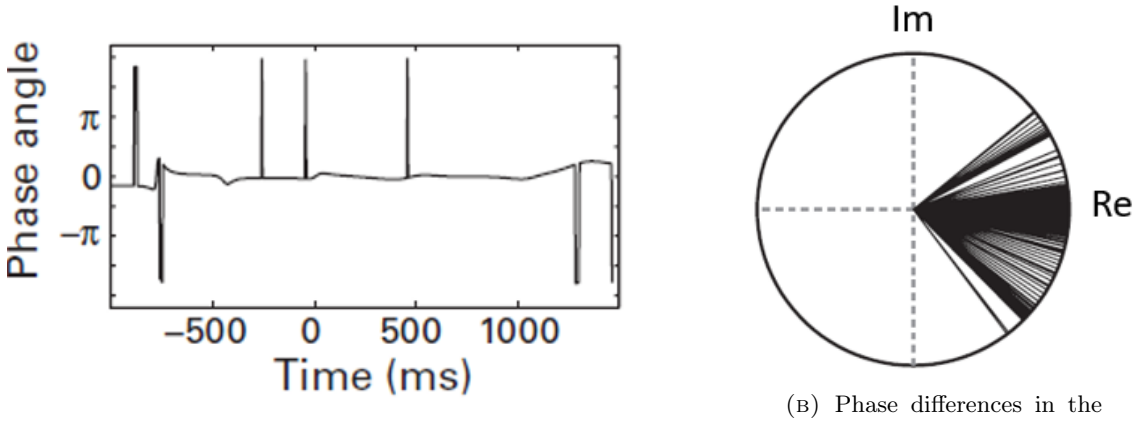

(A) Phase differences in time series [34].

(B) Phase differences in the complex plane.

FIGURE 5: On the left, the phase angle difference time series for signals x and y. On the right, the same phase angle differences over time are projected onto the complex plane. Figures taken from Cohen (2014) [34].

To do this, the average of these phase angle differences must be calculated. As phase angles are not on a linear scale, but a circular scale, we cannot simply add up the phase angles and divide by the number of measured phase angles [34]. For instance, consider phase angle differences of -0.1π and 2π, illustrated in figure 6 [36]. If averaged linearly, the answer would be 0.95π. However, on a circular scale, the answer should be -0.05π, as demonstrated by the yellow line in figure 6.

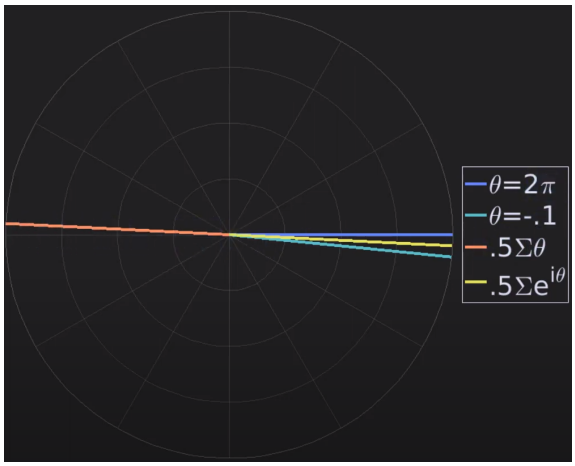

FIGURE 6: Example illustrating the problem with linear averaging of angles for signals x (in blue) and y (in green). The orange line represents the linear average, while the yellow line illustrates the correct circular average of the phase angles of x and y. Figure taken from Cohen (2019) [36].

This problem arises in particular with the use of $0/2\pi$. In general, averaging phase angles linearly leads to two possible answers, depending on the use of the sign. To address this, a solution is to average not just the phase angles themselves but the vectors representing these angles. This approach also provides insights into the concentration of data around specific phase angles. Without going into detail, averaging these vectors results in longer average vectors when individual angles are closely aligned. This outcome aligns with the concept of phase clustering (ISPC), the key

concept of most FC measures.

To demonstrate this with EEG data, an example is given when measuring signals from electrodes C3 and C4 (Figure 7). Here, the phase angle difference is calculated for the electrode pair C3-C4 for two timestamps t=0 and t=1 (Figure 7A). When averaging their corresponding vectors, an approximation is drawn with the blue line (Figure 7B) with a length of approximately 0.8.

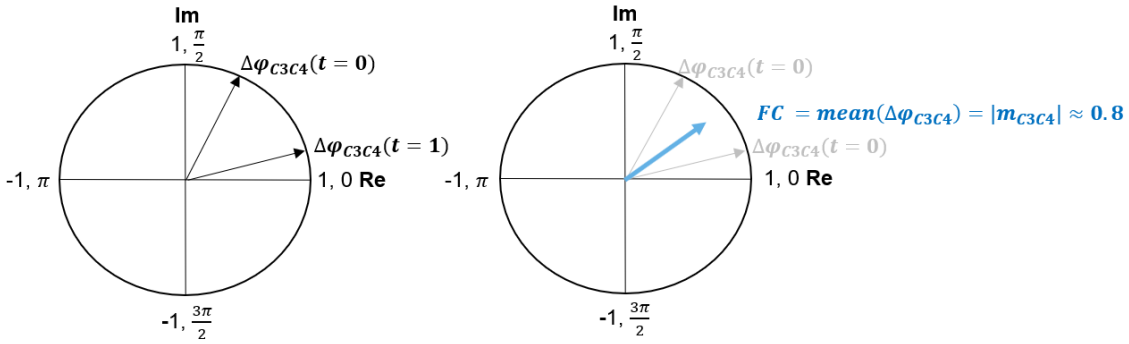

FIGURE 7: ISPC explained in polar space with a theoretical measurement of electrodes C3 and C4. On the left (A), two vectors with phase angle differences of two time points (t=0 and t=1): $\Delta\phi_{C3C4}(t=0)$ and $\phi_{C3C4}(t=0)$, respectively. On the right (B), the resultant averaged vector ($mean(\Delta\phi_{C3C4})$) of the vectors of both time points, corresponding to an amplitude of $|m_{C3C4}| \approx 0.8$.

Based on this information, we can describe the formula of ISPC (Equation 3), where we calculate this clustering of phase angle differences. This measure is essentially a summation of all data points n (over time t) of the previous equation (Equation 2) about the phase angle difference ($\phi_{x_t} - \phi_{y_t}$):

$$ISPC_f = \left| \frac{1}{n} \sum_{t=1}^{n} e^{i(\phi_{x_t} - \phi_{y_t})} \right| \tag{3}$$

Further explanation of variables of the equation

Here, $ISPC_f$ denotes the ISPC for a specific frequency f, computed as the absolute value of the average phase difference between the time points (t) of the brain signals x and y. The higher the clustering of phase differences, the higher the value of ISPC, ranging from 0 (no connectivity) to 1 (complete connectivity).

1.4.2 Volume conduction

Implementing ISPC to quantify FC can be problematic. This is due to volume conduction. Volume conduction (Figure 8 refers to the phenomenon where electrical signals spread almost instantaneously through the conductive medium (scalp, skull, and cerebrospinal fluid) surrounding the brain [34]. It is relatively instantaneous when considering that the electrical signal is traveling with the speed of light and only depends on factors such as the distance traveled, frequency, and resistance of the medium [37]. However, these factors only contribute to a very minimal delay compared to the electrical potential traveling from the brain region where some signal originates from the measuring electrode at the scalp. This relatively instantaneous transmission within the purpose of measuring true brain connectivity can lead to a spurious estimation of FC between brain regions, as the signals measured at different electrodes may reflect shared noise rather than neural communication.

As can be seen in Figure 8B and C, one brain signal can be detected by two electrodes due to instantaneous transmission [34]. This would then be detected as a phase angle difference of (almost) 0 or π. Whether that would be 0 or π depends on the spatial relationship between the measuring electrodes and the neural source. To elaborate, in case the electrodes are placed on opposite sides

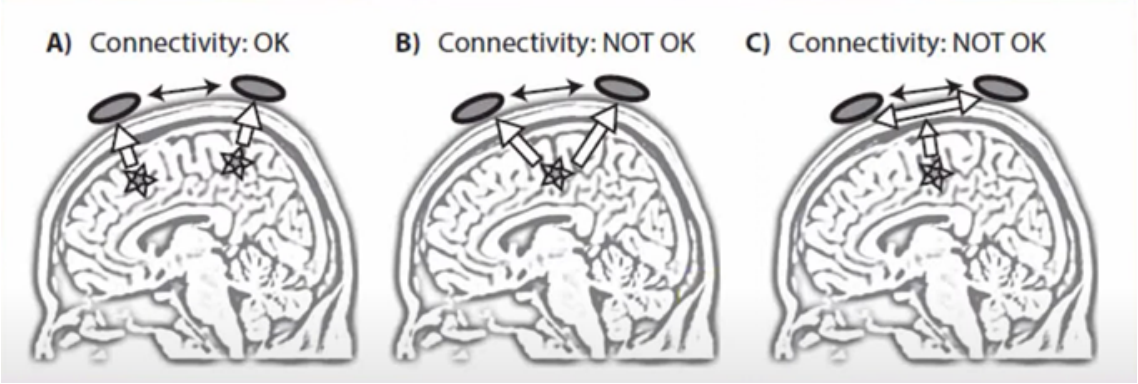

FIGURE 8: Volume conduction problem. Desired (A) and undesired (B and C) measured connectivity scenarios [34].

of the dipole, the measured signals exhibit a phase difference of π due to the inverse polarity [37]. Conversely, if the electrodes are on the same side of the dipole, a phase difference of 0 is observed due to aligned polarity.

That being said, true connectivity with a phase-lag of 0 or π does exist [34]. However, as explained here, there is a high chance that these values for phase-lags are related to volume conduction. Therefore, FC measures are preferred that exclude connectivity related to zero/π phase-lag.

In Figure (5b) we see phase clustering around a phase angle difference of 0. When quantifying FC with ISPC, it would generate a relatively high FC value, while in reality, this is probably due to volume conduction. To address this issue, the concept of weighting FC was introduced. This concept will be described in the next subsection.

1.4.3 Phase-lag-based FC measures

Vinck et al. [38] proposed measuring FC by a weighted Phase Lag Index (wPLI) in 2011. Before explaining wPLI, the Phase Lag Index (PLI) must be explained, a measure introduced by Stam et al. in 2007 [39]. Compared to ISPC, it is necessary to perform two additional steps to calculate the PLI. The first step is taking the imaginary part (See Figure 9):

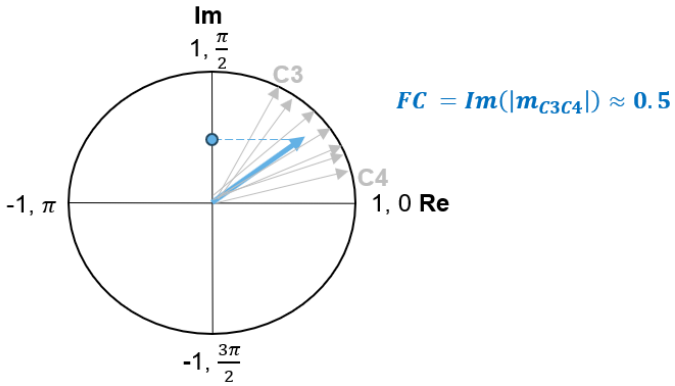

FIGURE 9: An example of 7 measured phase angle differences of electrodes C3-C4, with the average vector depicted in blue. Taking the imaginary part results in an FC value of approximately 0.5.

Similarly to Figure 7, the blue vector represents the averaging of phase angles. When taking the imaginary part of this vector value, the vector is projected onto the imaginary axis, indicating an FC value of approximately 0.5.

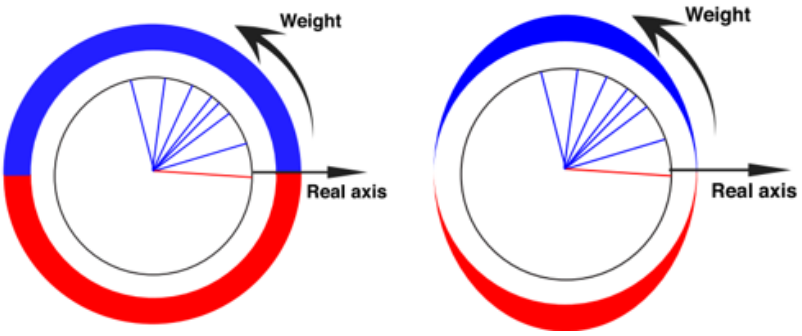

FIGURE 10: Concept of weighting FC. On the left weighting all phase-lags equally and on the right avoiding and diminisihing FC values when originating from a phase-lag difference around 0 or π. Figure taken from Vinck et al. (2011) [38].

The second additional step is taking into consideration the sign. That is, after taking the imaginary part, a value of 1 is assigned for positive phase differences and -1 for negative phase differences. In the example of figure 9, this FC value would be equal to 1. Hence, PLI computes the average sign of the imaginary part of the cross-spectral density (related to phase clustering), rather than averaging vectors [34]. In addition, the absolute value is taken as again, with functional connectivity, no difference between phase lag and phase lead is made. These steps together provide the following formula for PLI:

$$PLI = \left| \frac{1}{n} \sum_{t=1}^{n} \text{sign}(Im(S_{xyt})) \right| \quad \text{with} \quad S_{xyt} = e^{i(\phi_x - \phi_y)t} \tag{4}$$

Here, we have a summation with n data points over t time and S_{xyt} presenting the phase angle difference over time of signals x and y. As demonstrated by the equation, PLI quantifies the bias of phase angle differences towards either the positive or negative sides of the imaginary axis on the complex plane. A high PLI indicates that all phase angle differences are consistently on one side of the imaginary axis. Conversely, a PLI of zero signifies an equal distribution of positive and negative phase angle differences relative to the imaginary axis.

The wPLI builds upon the principles of PLI by incorporating weighting, based on the distance of the phase angles from the real axis [34, 38]. Equation 4 demonstrates that the wPLI not only considers the sign of the angles but also scales them by the magnitude of the imaginary component. Consequently, angle differences further away from zero or π radians exert a greater impact on the estimation of connectivity, as depicted in Equation 5. As a consequence, this creates the weighting as depicted earlier in figure 10.

$$wPLI = \frac{n^{-1} \sum_{t=1}^{n} |Im(S_{xyt})| \, \text{sign}(Im(S_{xyt}))}{n^{-1} \sum_{t=1}^{n} (Im(S_{xyt}))} \quad \text{with} \quad S_{xyt} = e^{i(\phi_x - \phi_y)t} \tag{5}$$

There is one thing to take into consideration when applying a weighting factor like in wPLI (by means of taking the imaginary part), compared to the more straightforward measure ISPC. At times, functional connectivity (FC) exhibits a phase-lag that gradually changes over time. For instance, if one signal oscillates at 10 Hz and another at 10.1 Hz, they synchronize, but their phase-lag slightly fluctuates over time (the averaged vector in polar space rotates with 0.1 Hz). Cohen et al. demonstrated this phenomenon through simulation [34] in Figure 11.

In this simulation (where nearly complete FC was simulated), ISPC was found to be consistent nearing 1, but debiased wPLI (dwPLI) was going to zero when the phase-lag passes 0 (or π). In conclusion, this simulation demonstrates once more the downside of using a phase-lag-based FC measure to avoid volume conduction, which is missing true connectivity.

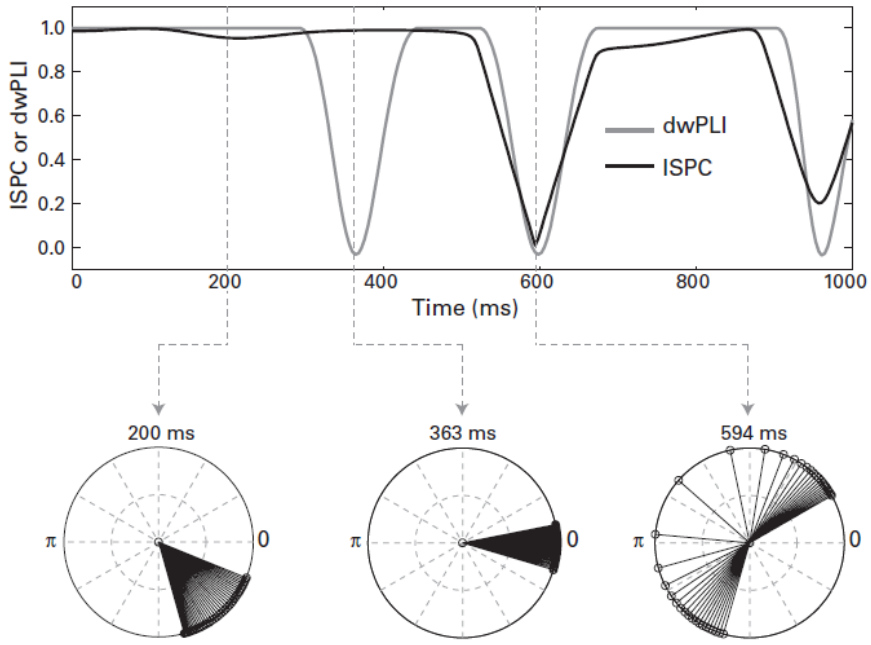

FIGURE 11: Simulation of detecting FC problem with phase-lag-based FC measure (dwPLI) when true FC occurs but is not stationary over time [34] At t=200 ms both dwPLI and ISPC detect correctly FC, but at t=363 ms, dwPLI misses true FC, while ISPC finds it.

1.4.4 Phase-lag and amplitude-based FC measures

PLI and wPLI assume equal amplitudes for all measurements. On the contrary, coherence based FC measures do not make this assumption and therefore include power (i.e. amplitude squared) information [34, 40].

Interestingly, Nolte et al. [40] claim that based on their study about quantifying FC with ImCoh, including the amplitude information yields more robust results. This may be due to the dependence of the phase-lag on the amplitudes. First, for a signal with low amplitude, it is more likely that its phase component would be distorted by noise [40]. Therefore, the measurement of signals with low amplitude would be less reliable, and therefore a weighting of the amplitudes would be desirable. Secondly, the measurement of phase angles is subject to a principle of uncertainty concerning amplitude size [35]. Specifically, smaller amplitudes introduce greater uncertainty in phase value determination, whereas larger amplitudes afford greater certainty in phase estimation. An analogy that comes to mind is measuring an angle using a geometric triangle. When trying to precisely determine a certain angle, opting for a longer distance from the angle being measured results in greater precision compared to a shorter distance. Similarly, when determining an angle of a signal's vector, a larger amplitude provides a more reliable determination of the phase angle. Thus, although the main objective is to assess a change in connectivity based on consistent phase measurement, incorporating the amplitude may enhance the reliability of these phase measurements ([40]).

The difference between purely phase-lag-based FC measures and both phase-lag and amplitude-based FC measures is illustrated in Figure 12. Here, in both the purely phase-lag-based example and the phase-lag and amplitude-based example, we can find vectors of two time stamps (t=0 and t=1) corresponding to the measured connectivity of electrode pair C3-C4. The phase angles are exactly the same, however, in the phase-based example we can see the equal amplitudes assumption, as all vector lengths are equal to 1. On the contrary, in the phase- and amplitude-based example, we find varying vector lengths, demonstrating the incorporation of amplitude information. For both types of FC measures, the imaginary part is used to handle the volume conduction. For example in the category of phase-based FC measures, wPLI uses the imaginary part and in the

category of phase- and amplitude-based FC measures, ImCoh explicitly makes use of this [38, 40]. To compare such measures, a projection onto the imaginary axis is made for both types of FC measures. Figure 12 shows that this leads to a (slightly) different outcome in measured FC.

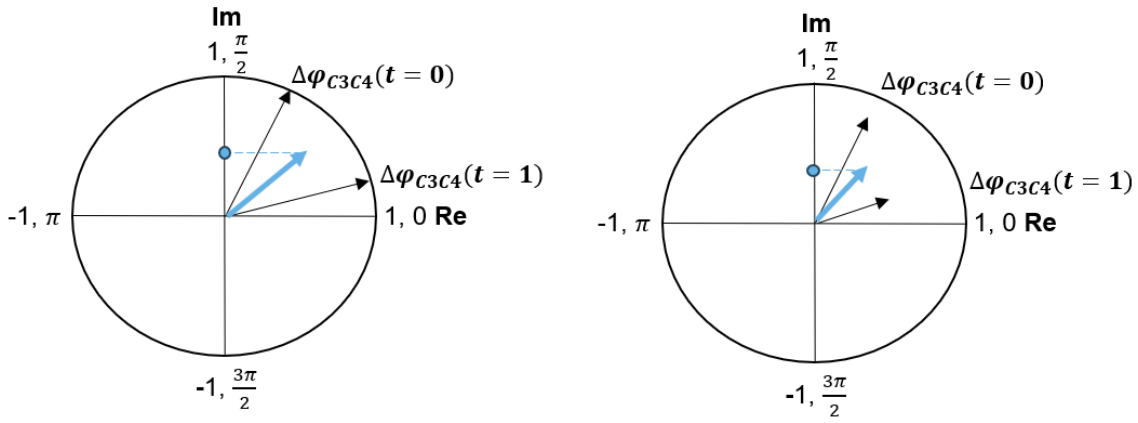

FIGURE 12: Difference between two categories of FC measures: purely phase-based (left) where the vectors are all equal to 1 and phase- and amplitude-based (right) where the vectors have varying amplitude. The blue vector is the average of both vectors originating from a phase-lag between two electrodes, in this example C3-C4. In addition, the projection to the imaginary axis is added for comparison of the two types of FC measures when both include only the imaginary part (e.g. wPLI and ImCoh).

Coherence-based FC measures are the most common practice within the type of incorporating both amplitude and phase components to measure FC. Coherence-based FC measures originate from the formula for coherency [40]:

$$C_{xy} = \frac{S_{xy}}{\sqrt{S_{xx}(f)S_{yy}(f)}} \tag{6}$$

with electrodes x and y. S_{xy} is the cross-spectrum and equation 6 the normalized cross-spectrum between x and y (normalized by auto-spectra of electrodes x and y). In more detail, S_{xy}, S_{xx} and S_{yy} can expressed as:

$$\begin{aligned} S_{xy} &= \langle m_x e^{i\phi_x} * m_y e^{-i\phi_y} \rangle = \langle m_x m_y e^{i\Delta\phi} \rangle, \quad \text{with} \quad \Delta\phi = \phi_x - \phi_y, \\ S_{xx}(f) &= \langle m_x e^{i\phi_x} * m_x e^{-i\phi_x} \rangle = \langle m_x^2 \rangle, \\ S_{yy}(f) &= \langle m_y e^{i\phi_y} * m_y e^{-i\phi_y} \rangle = \langle m_y^2 \rangle. \end{aligned} \tag{7}$$

In which $\langle\rangle$ represents an average over multiple EEG measurement time points. Here we find for

Filling this into equation 6, then it can be rewritten as:

$$C_{xy} = \frac{\langle m_x m_y e^{i\Delta\phi} \rangle}{\sqrt{\langle m_x^2 \rangle \langle m_y^2 \rangle}} \tag{8}$$

To go from coherency to coherence (Coh), the absolute value of $C_{xy}(f)$ is taken:

$$Coh_{xy}(f) \equiv |C_{xy}(f)| \tag{9}$$

When applying the absolute and take the square of m_x^2 and m_y^2, we get:

$$Coh_{xy} = \frac{|m_x m_y e^{i\Delta\phi}|}{|m_x||m_y|} \tag{10}$$

Then, if we take the imaginary part and translate this onto a scale over time points t, we get a formula that is similar to the format of ISPC (Equation 3) and wPLI (Equation 5). We then obtain Equation 11 [34]:

$$|ImCoh| = \frac{\left|Im(n^{-1}\sum_{t=1}^{n}|m_{tx}|\,|m_{ty}|\,S_{xyt})\right|}{n^{-1}\sum_{t=1}^{n}m_{tx}\cdot n^{-1}\sum_{t=1}^{n}m_{ty}} \quad \text{with} \quad S_{xyt} = e^{i(\phi_x-\phi_y)t} \tag{11}$$

1.4.5 Choice of FC measure

In this study, we have selected one phase-lag-based FC measure and one measure that incorporates both phase-lag and amplitude information. Specifically, we have chosen FC measures that are maximally robust against volume conduction. These measures are wPLI (a phase-lag-based FC measure) and ImCoh (a phase-lag and amplitude-based FC measure), as they both incorporate weighting along the imaginary axis such that spurious connectivity with phase-lag 0 and π is omitted.

When comparing ImCoh and wPLI, it is evident that they share a common foundation in phase clustering, as both include $e^{i(\phi_x-\phi_y)t}$. However, they diverge in two key aspects. Firstly, ImCoh does not take into consideration the sign simplification. Secondly, a significant distinction lies in the normalization of phase clustering (S_{xyt}) by the amplitudes of x and y. However, in the application of tACS when weak electric fields are used, no significant changes in power (amplitude squared) are expected [15, 41]. Returning to Nolte et al.'s assertion [40] that incorporating amplitude could enhance reliability due to increased weight on larger vectors and therefore higher reliability of measured phase values [40], this may not directly apply within tACS experiments. Thus, it can be concluded that ImCoh and wPLI should yield similar results in tACS experiments.

1.4.6 Impact of dual-site tACS phase lag on FC

Previous studies suggest that the manipulation of the induced phase lag in dual-site tACS might influence FC modulation. As discussed earlier (1.3), these studies have explored the effects of in-phase and anti-phase stimulation and typically reported a modulation of the FC compared to a sham condition. The dual-site tACS studies that have compared phase lag conditions [9, 10, 12–15, 29], assessed by offline FC data, are presented in Table 1.

TABLE 1: Dual-site tACS studies that have investigated at least in-phase and anti-phase conditions by means of an FC measure. Alongside, the frequency band of interest, FC measurement, and the primary FC outcomes were reported. FC measures used were wPLI, wPPC (weighted pairwise phase consistency), PPI (psychophysiological interaction), ImCoh, and MSC.

Study	**Frequency**	**FC Measure**	**Primary FC Outcome**
Meng (2023) [12]	beta	wPLI	Increased IP compared to AP and sham
Zhang (2023) [29]	alpha	wPPC	No change for any condition
Tan (2022) [13]	beta	ImCoh	No change for any condition
Schwab (2019) [14]	alpha	ImCoh	Increased IP compared to AP and jittered phase
Violante (2017) [11]	theta	PPI	Increased IP & increased AP for different regions
Helfrich (2014) [15]	gamma	MSC	Increased IP & no change AP compared to sham
Strüber (2014) [10]	gamma	MSC	Increased AP & no change IP compared to sham
Polanía (2012) [9]	theta	wPLI	Increased IP compared to AP and sham

Overall, investigating the effects of the used phase lags in dual-site tACS on FC modulation represents a crucial area of research with significant implications for understanding the aftereffects of

dual-site tACS. By gaining a better understanding of these effects, future dual-site tACS experiments may help mitigate the high variability observed in current research findings [9, 10, 12–15, 29].

1.5 Aim

Our main objective in this study is to investigate the role of induced phase lags in dual-site tACS applied to both primary motor cortices (M1s). Specifically, we aim to assess in what way the type of induced phase lag contributes to changes in FC (increase or decrease) within these regions. That is, we want to compare each phase lag condition with sham and also compare each phase lag condition with each other. This investigation offers insights into the mechanisms contributing to the observed variability in dual-site tACS outcomes, potentially enhancing treatment efficacy in neurological disorders.

In addition, we want to have more insights on how to interpret FC measures and have an indication of what FC measure might be preferred to use in the context of dual-site tACS. Moreover, we want to understand better the influence of various parameter settings used within our study design on detecting FC modulation, as will be discussed in 2.7.

Thus, our main research question is: "How does the phase lag condition in dual-site transcranial Alternating Current Stimulation (tACS) induce changes in beta-band EEG functional connectivity (FC) between the primary motor cortices of healthy participants?"

In combination with the sub-questions:

- Which FC measure effectively captures the observed changes in FC?
- What parameter settings effectively capture the observed changes in FC?

Based on earlier findings [9–15, 29], we hypothesize that dual-site tACS will induce changes in functional connectivity (FC) across different phase lag conditions. Given the variability in outcomes from previous studies, we do not hypothesize whether these changes will manifest as increases or decreases in FC. Instead, we hypothesize that different phase lags will result in distinct changes in FC. If a uniform distribution across the phase lags is observed, we expect this will be evident in the polar plot, with one or more phase lag conditions showing lower or higher ΔFC values compared to Sham.

In addition, we hypothesize that both imaginary coherence (ImCoh) and weighted Phase Lag Index (wPLI) effectively capture the observed changes in FC. While variations in outcomes are anticipated due to the inclusion of amplitude weighting in ImCoh and its exclusion in wPLI, it is expected that both measures yield comparable results, aligning with the main research question.

2 Methods

2.1 Participants

Nine healthy participants between the ages of 18 and 34 years (mean age: 26) were recruited for this study and received financial compensation. Of these participants, six were male and three were female. Additionally, six were right-handed, and three were left-handed. No participant had undergone brain stimulation before. Prior to the experiment, participants were provided with detailed information about the study procedures and objectives, after which they provided written informed consent. The study was approved by the ethical committee of the University of Twente, Faculty of Electrical Engineering, Mathematics, and Computer Science (EEMCS) and was conducted according to the declaration of Helsinki (2013).

2.2 Experimental design

In this study, dual-site tACS was performed using four different phase-lags, namely 0 (IP: InPhase), $\pi/2$ (PH: PiHalf), π (AP: AntiPhase), and $3\pi/2$ (3HP: 3HalfPi). Additionally, a sham condition was included, this condition tries to replicate the sensory experience of tACS stimulation without administering actual electrical stimulation. Thus, in total each participant underwent all five conditions. For the four phase-lags and the sham condition, a ramp-up and ramp-down of the stimulation, with a duration of 3 seconds each, were used.

FIGURE 13: Experiment set-up for one condition of one participant. During stimulation blocks are white, the pre-stimulation block is marked in blue, post-stimulation blocks are marked yellow (post-stimulation block right after first stimulation dark yellow) and the no-stimulation block is marked green.

Each condition consists of a 22 minute block (see Figure 13). The data can be divided into during stimulation (white), pre-stimulation (blue), post-stimulation (yellow) data and no-stimulation (green). EEG data was acquired during all the blocks of each condition. Nevertheless, the EEG data during stimulation (online data) is heavily influenced by the tACS stimulation [42], so this data is filtered out during preprocessing. For the analysis we only used the data before and after stimulation, specifically, pre-stimulation and post-stimulation blocks (offline data). The no-stimulation block has been excluded from the analysis to ensure consistent block lengths for all data right after a stimulation block.

The order of the conditions was randomized for each participant, and they were blinded to the order. Moreover, there was at least a 5-minute interval between each condition. This is considered to be sufficient rest such that we can assume independence between conditions within one subject.

2.3 Electrophysiological recordings and stimulation

The raw multichannel data derived from the experiment with dual-site tACS, consists of recordings of all nine participants. The multichannel data contains 64 measuring EEG electrodes (with FCz as the reference electrode), 8 stimulating EEG electrodes, 4 EoG electrodes, and 2 ECG electrodes.

In the experimental setup, a weak electrical current of 4 mA peak-to-peak, 20 Hz, to both primary motor cortices (M1s) using dual-site tACS was administered. The alternating current is generated by employing a 3 to 1 electrode montage. This montage consists of a central stimulating electrode where a maximum current of 4 mA is applied, surrounded by three outer electrodes with an opposite current of 1/3 of the value of the central electrode each one, which serve as counterbalances to prevent current leakage.

In Figure 1, found in Section 1.1, an illustration of a 4 to 1 electrode configuration was provided for reference. The primary distinction between this montage and the one we used lies in the presence of a fourth outer electrode near the ear in the 4 to 1 configuration, which is absent in our 3 to

1 system. Additionally, it is worth mentioning that the relative distances between the electrodes and their sizes depicted in the figure are exaggerated for visualization purposes. Nevertheless, the figure effectively elucidates the underlying principle, highlighting the central electrode (in red) delivering positive current and the surrounding outer electrodes (in blue) responsible for delivering an opposite current to maintain focus on the targeted stimulation site and prevent current leakage.

This targeted stimulation site is the M1 on both hemispheres. Specifically, for this study the cental stimulation electrodes were positioned in the EEG positions C3 on the left M1 and C4 on the right M1. The corresponding outer electrodes were FC3, C1, CP3 and FC4, C2, CP4 on the left and right M1, respectively. Each set of four electrodes then creates an electric field underneath.

In figure 14, the set-up of EEG electrodes is shown, of which the green and yellow marked electrodes follow the 10-10 electrode system for EEG recording [43]. However, the green and yellow electrodes with the black outline are not used for measuring the EEG but for the tACS stimulation. Therefore, an additional eight electrodes are placed nearby the stimulation electrodes. Following the arrow from the black outlined electrodes to a red or white electrode, around the left primary motor cortex we use the additional measuring electrodes CCP5h, FFC5h, FCC3h, CCP3h. Around the right primary motor cortex we use the additional measuring electrodes CCP6h, FFC6h, FCC4h, CCP4h.

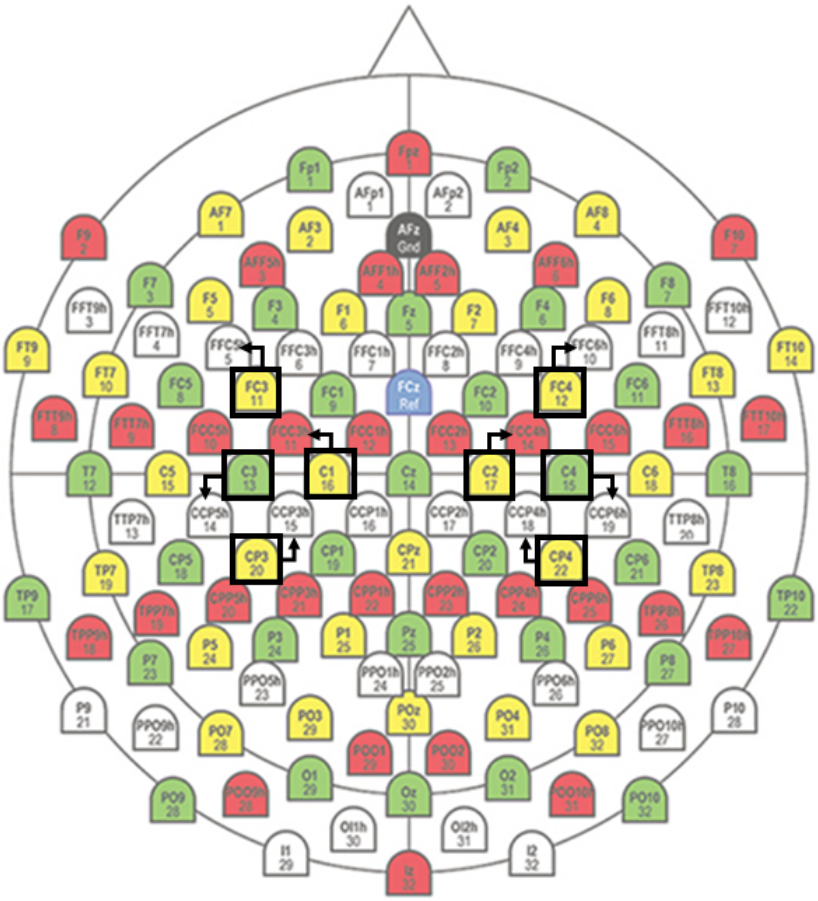

FIGURE 14: Configuration of the 10-10 electrode system for EEG recording, figure taken from Brain Products GmbH [44]. Green and yellow electrodes represent the standard 10-10 layout. Optional red and white electrodes are utilized for setting up 4-to-1 tACS montages in the M1 region bilaterally. These stimulation montages, outlined in black, are solely for delivering stimulation and do not record EEG data. Eight arrows originating from the outlined electrodes indicate which nearby red or white electrodes are used instead for EEG measurement. The black electrode AFz serves as the ground electrode and the blue electrode FCz as the reference electrode.

2.4 Data pre-processing

The recorded data was subjected to the following preprocessing steps:

1. Data division into online and offline data;
2. Concatenation of offline data;
3. Bandpass filtering 0.5-40 Hz;
4. Downsampling from 5 kHz to 2.5 kHz;
5. Application of Independent Component Analysis (ICA). ICA decomposes EEG signals into statistically independent components, which we can use to eliminate physiology-based artifacts;
6. Pearson's linear correlation was employed to compare ICA components with electrocardiography (ECG) and electrooculography (EOG) signals. Thresholds were initially set at 0.2 for both EOG and ECG, in accordance with a previous dual-site tACS experiment by Schwab et al. [14]. Following analysis of pilot data, the threshold for ECG was adjusted to 0.3;
7. Additional ICA components based on visual inspection were removed [45]. Components where frontal focused activity was observed were identified as EOG related components and therefore eliminated. Electromyography (EMG) related data was recognized by focalized activity around the ears or neck. Additionally, characteristic muscle-like activity patterns were identified through inspection of the Power Spectral Density (PSD) plots [34]. By integrating topographic plot inspection with analysis of the PSD plot, muscle-related artifacts were effectively removed. In total, no more than five ICA components were removed to ensure sufficient preservation of data;
8. In the ICA processing step, additional components were visually inspected and removed to preserve data quality. Electrooculography (EOG) channels were examined for frontal-focused activity indicative of eye movements. Electromyography (EMG) related data was identified through focalized activity around the ears or neck in combination with Power Spectral Density (PSD) plot inspection for typical muscle-related artifacts, ensuring their removal. To maintain data integrity, a maximum of five components were removed, balancing artifact removal with data preservation;
9. Identification and removal of noisy channels were conducted. Channels with an average amplitude exceeding three times the standard deviation of the mean amplitude across all channels were automatically excluded from further analysis. In addition, further channels were excluded from analysis based on real-time observations during data acquisition and post-experiment inspection;
10. To ensure consistency in the number of channels across all participants, eliminated channels were interpolated. Interpolation is a technique used to estimate the missing data points by averaging the neighboring electrode signals. This process ensures that each participant has the same number of channels for analysis;
11. Re-referencing the EEG data to an average reference. This involves calculating the average signal across all electrodes and subtracting this average signal from each individual electrode. This step is performed to create a new reference point that helps eliminate common noise sources from the EEG signals.

2.5 FC analysis

Offline data were analyzed for all 9 participants to identify changes in FC. For the pre-stimulation data, we use the 3-minute block preceding the first 5-minute stimulation block (highlighted in blue in Figure 13). This 3-minute EEG data is divided into multiple segments, such as 9 segments of 20 seconds. The number of post-stimulation segments used, dependent on the post-stimulation averaging type (see 2.7.1), was also applied to the pre-stimulation data. For instance, if 6 segments were used for post-stimulation averaging, then the same number of segments (6) was selected for

pre-stimulation averaging. FC is calculated for each of the selected segments, and then the average FC value across the segments is computed and divided by the number of segments to obtain the final averaged FC value for the pre-stimulation EEG data. An example of this data division is illustrated in Figure 15.

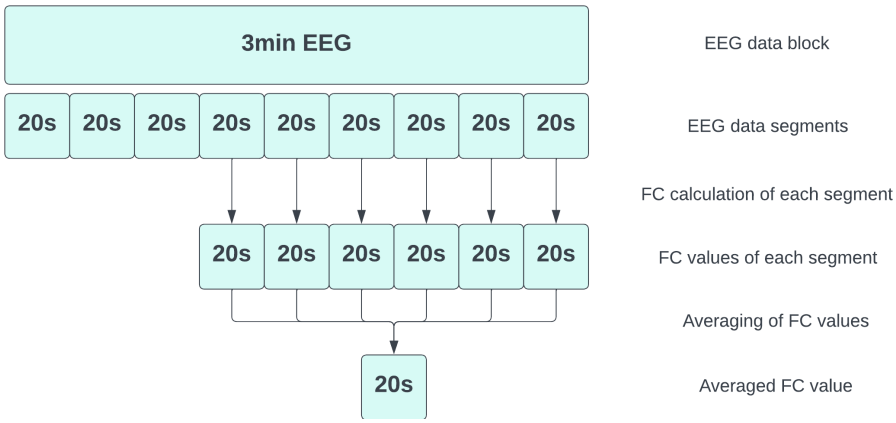

FIGURE 15: The pre-stimulation block, lasting three minutes, is divided into segments. In this example, segments of 20 seconds each are used, resulting in a total of 9 segments. FC is calculated using only the last 6 segments to align with the number of used post-stimulation segments (averaging type 1). The resulting FC values are averaged to obtain a single pre-stimulation FC value.

.

For the post-stimulation data, we have six 1-minute blocks following a stimulation period. The first block immediately follows a 5-minute stimulation period and is marked in darker yellow, while the subsequent five blocks follow 1-minute stimulation periods. From each 1-minute block, initially the first segment right after stimulation is derived. For further inspection of changes in FC over time, other segments are also used, further explained in Section 2.9. For the six derived segments of, for example, 20 seconds, the FC values are calculated from the EEG data of each segment. Then, for most of the analysis (see other averaging types in Section 2.7.1), the average of all segments is calculated. In the end, we obtain one averaged post-stimulation value.

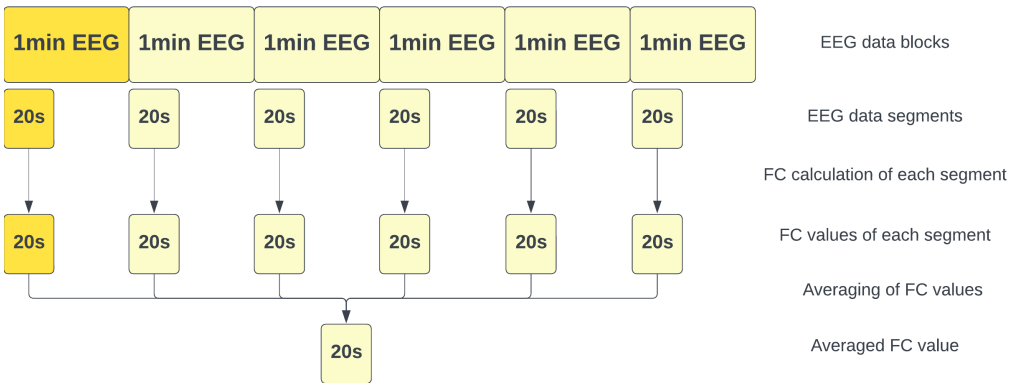

FIGURE 16: The post-stimulation data is derived from six one-minute blocks. In this example, a segment length of 20 seconds is used. Additionally, from each one-minute block, the first segment of 20 seconds is selected. FC is then calculated for each of these six segments, and the resulting FC values are averaged to obtain a single averaged post-stimulation FC value.

.

From this averaged post-stimulation segment FC value and the averaged pre-stimulation FC value, we can quantify the change in FC as depicted in Equation 12:

$$\text{Change in FC} = \text{post-stimulation FC} - \text{pre-stimulation FC} \tag{12}$$

The whole experiment design from preprocessing to calculating the change in FC can then be summarized in the following flowchart (Figure 17):

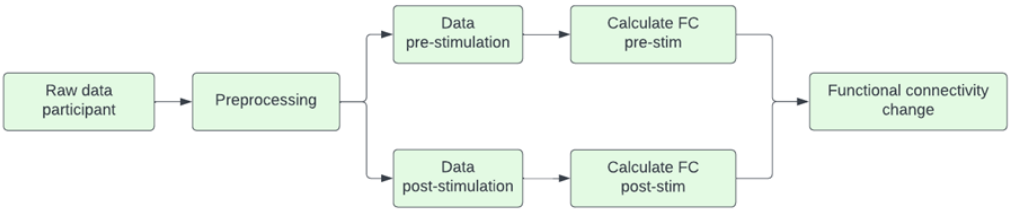

FIGURE 17: Flowchart of experiment design.

.

2.6 FC measures

FC was computed at the electrode level using two connectivity measures: ImCoh and wPLI. This study aims to elucidate the distinctions in outcomes between these two measures. To achieve this, we initially focus solely on the pre-stimulation data. This approach isolates the influence of stimulation, allowing us to evaluate the differences between the two measures independently. We will examine whether they exhibit similar baseline values and variance, and if they manifest comparable variability across the five conditions.

Subsequently, the results regarding the change in FC will be compared. The primary emphasis lies in determining whether the observed changes in FC are consistent and comparable between the two FC measures. Specifically, the objective is to determine whether these measures lead to similar conclusions regarding our primary research question.

2.7 Parameter settings

In this study, we explore various parameters crucial for calculating FC. These parameters include: the type of averaging used for post-stimulation data, epoch length, frequency band, and EEG electrode pairs. Table 2 provides a summary of the different settings investigated for each parameter. Initially, a base setting is chosen for each parameter, which serves as the basis for the final result — the primary outcome addressing the main research question concerning the influence of various (phase lag) conditions on the change in FC after dual-site tACS.

Subsequently, to address the research subquestions, we examine how alterations in each parameter setting might affect the observed changes in FC. By comparing these variations with the main result, our analysis aims to identify the most effective settings for highlighting changes in FC. The insights gained can guide the selection of optimal FC analysis configurations for future studies.

2.7.1 Averaging post-stimulation blocks

FC values are known to be fluctuating over time [46–48]. Therefore, the experiment is designed such that we can use multiple post-stimulation blocks to subsequently average the FC values of these post-stimulation blocks. There are 6 post-stimulation blocks of one minute long in the experiment. Throughout the analysis, three different types of averaging the post-stimulation blocks were tested: averaging type 0, type 1 and type 2. For these blocks, first the FC was measured per block, to then average their FC values such that we have one averaged post-stimulation FC value.

For averaging type 0, only the initial post-stimulation block is used, indicated by its darker yellow shade compared to the subsequent 1-minute post-stimulation blocks (refer to Figures 13 and 16). Therefore, with averaging type 0, no averaging across multiple blocks is performed. This specific

TABLE 2: FC measuring parameters and its settings. Base settings are marked in bold.

Parameters	Settings
Type of averaging the post-stimulation blocks	Averaging type 0: No averaging, use only the first epoch after the first block of 5 minute stimulation **Averaging type 1**: Average all six epochs (use all post-stimulation epochs) Averaging type 2: Average last five epochs (only use epochs after a 1 minute stimulation period, exclude epoch after 5 minute stimulation)
Epoch length	12 seconds **20 seconds** 30 seconds
Frequency band	13-30 Hz 15-25 Hz **17-23 Hz** 19-21 Hz
Electrode pairs (averaging)	CCP5h-CCP6h FFC5h-FFC6h FCC3h-FCC4h CCP3h-CCP4h C5-C6 **Average of all 5 electrode pairs around M1**

block is of particular interest as it immediately follows the first and longest stimulation period of the experiment.

Averaging type 1 is where all six 1 minute post-stimulation blocks are used to assess the change in FC. Averaging type 2 is where all six but the first 1-minute post-stimulation blocks are used, so in total five 1-minute blocks (all five light yellow blocks) are used and averaged. We have these distinct averaging types, as the first stimulation block of 5 minutes is longer than the other 1 minute stimulation blocks, which could have an effect on the measured post-stimulation data.

For the general (change in) FC analysis, we picked averaging type 1. This is because we then use all post-stimulation blocks to have the most robust averaged FC data. Using multiple post-stimulation blocks allows us to capture a broader range of temporal dynamics and potential fluctuations in FC over time. By averaging across these blocks, we mitigate the influence of any individual block's variability or outlier data points, resulting in a more stable and reliable representation of the overall change in FC following stimulation.

2.7.2 Epoch length

Research on the impact of epoch length on the measurement of FC is scarce, with only a couple of studies exploring its effects on EEG data analysis [49–51]. Fraschini et al. [49] investigated the influence of epoch length on PLI and amplitude envelope correlation (AEC). Our focus lies primarily on PLI due to its relevance to our study, which employs a similar phase-lag-based measure, wPLI. Notably, they observed that PLI stabilizes around 8-12 seconds, with full stabilization occurring at approximately 12 seconds. Using an epoch length shorter than 8 seconds can result in excessively high connectivity, as illustrated in Figure 18.

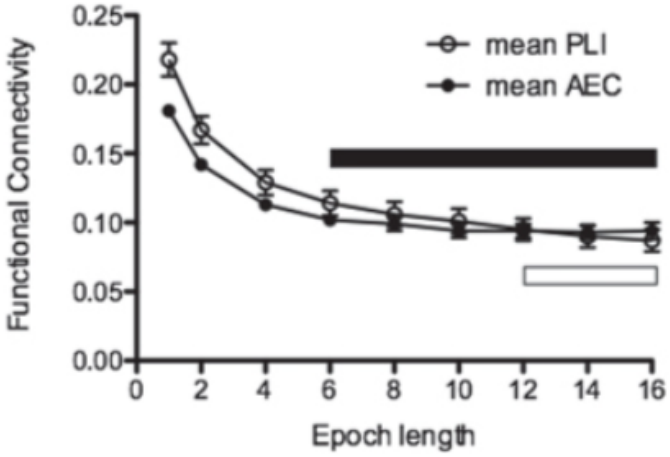

FIGURE 18: The influence of epoch length on the measured FC by PLI and AEC. PLI, the FC measure of interest, stabilizes around 8-12 seconds, being fully stable at 12 seconds. Figure taken from Fraschini et al. [49].

.

On the other hand, Chu et al. [50] suggest that FC measures may take up to 100 seconds to fully stabilize. This duration aligns with dual-site tACS-related studies that found a stimulation-outlasting effect for their first used epoch with a length of 100 seconds [10, 14]. However, in other scenarios, the stimulation-outlasting effect of dual-site tACS may be brief. Using an epoch length of this magnitude gives rise to the risk of overlooking the effect of tACS.

Furthermore, Tort et al. [51] investigated the effect of the epoch length on the statistical measure of assessing the modulation index (MI) for various phase bins. They found that for 30 seconds and longer, a stable MI was expected. Shorter than 30 seconds can lead to a spurious MI. They emphasize that these findings for MI are probably transferrable to other cross-frequency coupling (CFC) measures.

Ultimately, selecting an appropriate epoch length involves a trade-off. A shorter epoch length increases the risk of capturing spurious connectivity due to insufficient data samples, while a longer epoch length may obscure the effects of tACS. Based on these considerations, we opt to test epoch lengths ranging from a minimum of 12 seconds to a maximum of 30 seconds in our study.

2.7.3 Frequency band

Around the 20 Hz frequency stimulus, investigation into the beta-band FC is conducted. Typically, the beta-band encompasses frequencies ranging from 13 to 30 Hz. Prior studies targeting the beta-band with tACS at 20 Hz have similarly explored the 13-30 Hz range [1, 12, 52] or closely to this range [13, 30, 53]. However, a critical question arises regarding the necessity of investigating such a broad frequency band when applying tACS at 20 Hz. It remains unclear whether the effects extend to frequencies at the edge of the beta-band (e.g. 13 Hz, 30 Hz) or primarily remain centered around 20 Hz. There is concern that by selecting a band that is too broad, the effect of tACS may be overlooked.

2.7.4 Averaging electrode pairs

We choose to study the following electrode pairs since these are found in the M1s and around them:

- CCP5h-CCP6h
- FFC5h-FFC6h
- FCC3h-FCC4h

- CCP3h-CCP4h
- C5-C6

From these selected electrode pairs, we are able to assess FC, as further elaborated in Section 2.5. One such electrode pair in proximity to the stimulation electrode pair C3-C4 is CCP5h-CCP6h. Given the possibility of a localized effect of tACS, we initially examine the FC values obtained from these electrodes. However, as mentioned before when averaging post-stimulation blocks (Section 2.7.1), FC values fluctuate over time due to dynamic brain activity [46–48]. Therefore, similar to averaging the post-stimulation blocks, we have additionally computed the average of FC values derived from all electrode pairs. This enhances the robustness of our FC calculations in assessing changes.

2.8 Statistics

Circular and linear statistical methods
To gain a comprehensive understanding of how the change in FC (ΔFC) varies across different phase lag conditions, we employed circular statistics for our analysis. This approach enables us to preserve the circular nature of the phase lags, allowing us to test our hypotheses. That is, we hypothesized that phase conditions like InPhase and AntiPhase, which exhibit opposite phase lags, would induce contrasting effects on ΔFC. Equivalently, this opposite relationship is expected between the PiHalf and 3HalfPi conditions.

Initially, we applied standard linear statistical methods in the form of an analysis of variance (ANOVA). However, we encountered limitations with this approach. ANOVA does not consider the circular nature of the data, leading to a loss of angular relationship between conditions. This loss of relationship could potentially mask a significant effect of tACS, particularly when opposite effects are anticipated across different phase lags. In an ANOVA F-test, the test statistic is evaluated against the overall mean. This can become an issue when more than one phase lag exhibits a significant change in FC. Possibly, a larger change in FC is needed to achieve significance compared to when only one phase lag deviates from the overall mean.

Even more, when employing circular statistics, any opposite effect across inverse phase lag conditions would be found for a relatively smaller change in FC. When two phase lag conditions display contrasting effects in ΔFC, the skewness of the circular distribution becomes more pronounced compared to the scenario where only one phase lag condition is affected by the stimulation. On the other hand, we have to keep in mind that this principle holds true in reverse. That is, if opposing phase lag conditions demonstrate the same type of change (e.g. both increased FC), then a relatively higher change in FC is required to be regarded as significant. Moreover, in a scenario where all phase lag conditions demonstrate a similar type of change in FC (distinctly different from ΔFC=0 and/or distinctly different from sham), the distribution remains uniform.

Mean Vector Length
In general, we choose circular statistics to preserve the angular relationship between the phase lag conditions. Specifically, we opted to use the Mean Vector Length (MVL) in conjunction with permutation statistics [54]. This method, also referred to as Amplitude Phase Locking (APL) [55], has been validated in the context of phase-amplitude coupling [51, 56]. In our study, rather than evaluating amplitudes for each phase condition, we examined changes in FC across various phase lag conditions. By integrating permutation statistics into this approach, we circumvented the need for a normal distribution and mitigated any potential shortcomings associated with MVL [56].

Multiple condition comparisons
If the null hypothesis is rejected, indicating a non-uniform distribution with a significant MVL at a p-value < 0.05, we will proceed with planned comparison testing. As outlined in our research plan, in the event of a notable non-uniform distribution of phase lags, our aim is to assess which phase lag condition significantly differs from the sham condition. In addition, we also aim to assess differences among the phase lag conditions. Therefore, we have designed multiple comparisons tests with all ten comparisons:

- SH-IP

- SH-PH
- SH-AP
- SH-3HP
- IP-PH
- IP-AP
- IP-3HP
- PH-AP
- PH-3HP
- AP-3HP

Given that the same participants are used for different conditions, a two-sample dependent test is used for the comparisons. Initially, the normality of the paired data will be assessed using the Shapiro-Wilk test [57]. If the data conforms to a normal distribution, we will use the parametric paired-sample t-test to assess the significance of differences in the two means. Alternatively, if the data deviates from normality, the non-parametric counterpart of the t-test for dependent samples will be employed i.e. the Wilcoxon signed-rank test. To address the issue of multiple hypothesis testing and control for false positives in our statistical analysis, we applied a Bonferroni-correction to the p-values obtained from our hypothesis tests.

2.9 Visualization of temporal changes in FC

After initially analyzing only the immediate segments of the post-stimulation blocks, the full post-stimulation block can be fully examined by implementing a sliding window approach to explore temporal changes in connectivity. This sliding window has the length of the chosen segment length. For instance, with an initial segment length of 0-20 seconds and a sliding window shift of 5 seconds, subsequent intervals would progress as follows: 5-25 seconds, 10-30 seconds, and so forth, up to 40-60 seconds, covering the entire minute of the post-stimulation block. By implementing this approach, it can be visualized how the measured change in FC behaves over time. However, no statistical significance is assessed for these additional segments beyond the initial 0-20 seconds time window.

2.10 Optimization of settings based on preliminary results

While analyzing the preliminary results of the base setting, we observed no statistically significant differences in either ImCoh or wPLI. Subsequently, in our initial exploration of all parameter settings, we identified a significant result for the electrode pair FCC3h-FCC4h (measured by wPLI). However, the significance of this finding was marginal and did not persist in subsequent multiple comparisons tests. This led to further exploration of the parameter settings for p-values close to significance ($p<0.10$).

Exploration of parameter settings within our preliminary results (see Table 3 in Section 3.1) provided the following findings:

- Electrode pairs: In addition to the significant electrode pair FCC3h-FCC4h, we found for C5-C6 a p-value below 0.10. Other electrode pairs used for EEG measurement were investigated adjacent to these electrode pairs (FCC3h-FCC4h, C5-C6) for relatively low p-values ($p<0.10$). This led to our finding that FC5-FC6 showed a significant result for 17-23 Hz.
- Frequency band: Broader frequency bands (15-25 Hz, 13-30 Hz) exhibited p-values below 0.10.
- Averaging type: The p-values exhibited little variation, which justifies retaining the averaging type that incorporates all data (averaging type 1).

- Epoch length: A substantial increase in the p-value was observed upon either decreasing (12s) or increasing (30s) the epoch length, thus indicating to maintain an epoch length of 20s.

Overall, after examination of each parameter setting individually, it suggested that a broader beta-band of 15-25 Hz or 13-30 Hz, and averaging across a different set of electrode pairs are desired optimizations within our parameter choices. Furthermore, preliminary results indicate that the optimal settings involve an epoch length of 20 seconds and averaging type 1, as utilized in the base settings.

The full beta-band encompassing 13-30 Hz was selected over the narrower range of 15-25 Hz, as this supports better comparability with prior beta-band studies. For example, for dual-site tACS studies regarding the effects on FC within the beta-band specifically, frequency bands of 13-30 Hz [12] and 14-33 Hz [13] were used.

In selecting electrode pairs, we opted to include those demonstrating significance or nearing significance ($p<0.10$) within the 13-30 Hz band, specifically the FCC3h-FCC4h, C5-C6, and FC5-FC6 pairs. This approach enhances the statistical power of the FC analysis.

3 Results

To facilitate a clear understanding of the findings, we introduce the structure of this results section. Initially, the preliminary results obtained using the base settings (as introduced in Section 2.7) are presented in Section 3.1. Subsequently, Section 3.2 details the results across all parameter settings. Based on these findings, we selected optimal settings, which are presented in the final results in Section 3.3.

3.1 Preliminary results with base settings

Change in FC: Individual data

The change in FC (ΔFC) is initially depicted in Figures 19a and 19b, measured by ImCoh and wPLI respectively. These figures provide insight into the spread of ΔFC across participants under each phase lag condition, offering an overview of the variability in response to dual-site tACS. In general, the figure facilitates a first examination of any trends within the dataset.

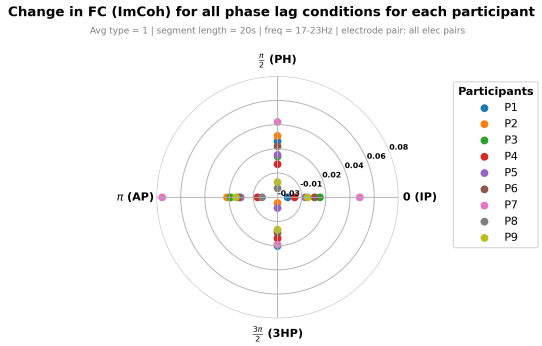

(A) ΔFC for ImCoh. Values range from approximately -0.03 (origin of the polar plot) to 0.08 (outer radius of the polar plot).

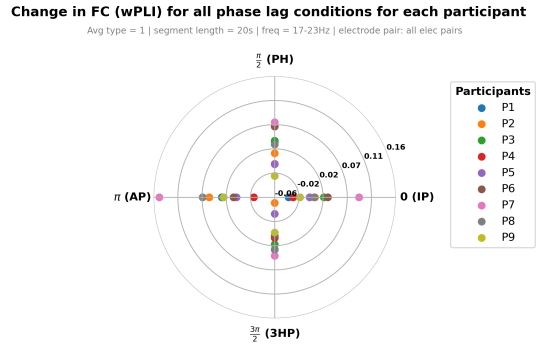

(B) ΔFC for wPLI. Values range from approximately -0.06 (origin of the polar plot) to 0.16 (outer radius of the polar plot).

FIGURE 19: The average change in FC (ΔFC) measured by ImCoh and wPLI during the initial 20 seconds following stimulation across four phase lag conditions: InPhase (IP, phase lag = 0), PiHalf (PH, phase lag = $\pi/2$), AntiPhase (AP, phase lag = π), and 3HalfPi (3HP, phase lag = $3\pi/2$). The dots within each phase lag condition represent the change in FC for each of all 9 participants. Base settings were used and described in the grey subtitle.

Change in FC: Means ±1 standard deviation

A second visualization of the dataset is presented in Figures 20a and 20b. Here, the individual data of the four phase lag conditions was transformed, such that each condition is represented by the mean value and its corresponding ±1 standard deviations. This allows for a more comprehensive overview of the data in an attempt to visualize any possible non-uniform distribution across the phase lags. In addition, the sham data was added for direct comparison with all four phase lag conditions.

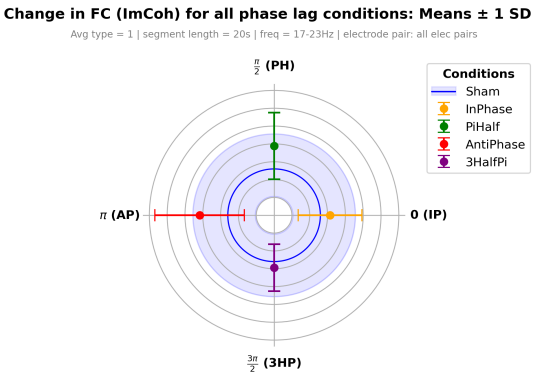

(A) ΔImCoh for all phase lag conditions: means ±1 standard deviation.

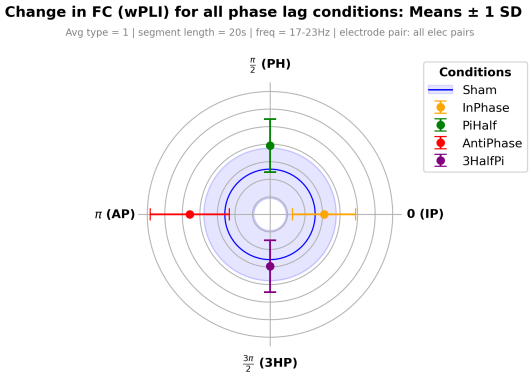

(B) ΔwPLI for all phase lag conditions: means ±1 standard deviation.

FIGURE 20: ΔFC measured by ImCoh and wPLI for all phase lag conditions, with the error bars representing the means (dot) from all 9 participants, +1 standard deviation from the mean (outer cap) and -1 standard deviation from the mean (inner cap). The blue circle represents the mean and the blue shaded region represents its ±1 standard deviation spread. Base settings were used.

Mean Vector Length

In Figures 21a and 21b, the average ΔFC over all nine participants for each of the phase lag conditions is depicted, represented by the length of the vector. The Mean Vector Length (MVL) is computed from these phase lag vectors, providing a measure of the overall directionality and strength of phase preference across conditions. To enhance visibility, the MVL is magnified by a factor of 4, ensuring a clear illustration of the MVL. The primary role of the MVL is to act as the test statistic for evaluating the uniformity of distribution across phase lags; a relatively small MVL implies uniform distribution, while a relatively large MVL indicates non-uniform distribution. Permutation statistics are employed to objectively assess whether the length of the MVL is significant.

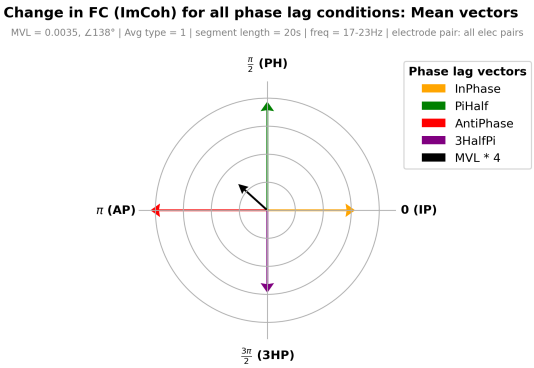

(A) ΔImCoh for all phase lag conditions: phase lag vectors and Mean Vector Length.

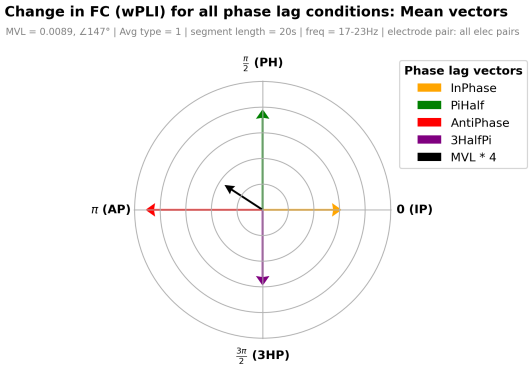

(B) ΔwPLI for all phase lag conditions: phase lag vectors and Mean Vector Length.

FIGURE 21: Comparison of changes in FC across various phase lag conditions using ImCoh and wPLI measures. Each colored vector represents the mean of a specific phase lag condition. The black vector represents the MVL, enlarged by a factor of 4 for illustrative purposes. Base settings were used.

Permutation statistics

Figures 22a and 22b illustrate the null hypothesis distribution of MVL across 10,000 iterations, represented by the blue bars distributed over 50 bins. The selection of 10,000 iterations was determined empirically to ensure the stability of the statistical values for each run.

The observed MVL yields p=0.360 for ImCoh and p=0.150 for wPLI. Consequently, the null hypothesis cannot be rejected, suggesting a uniform distribution across the four phase lag conditions.

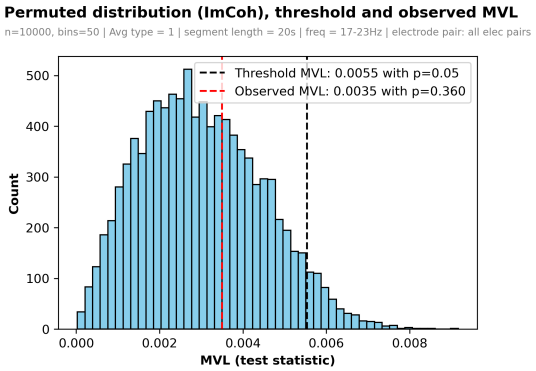

(A) Permuted distribution for ImCoh with the observed MVL correlating to p=0.360.

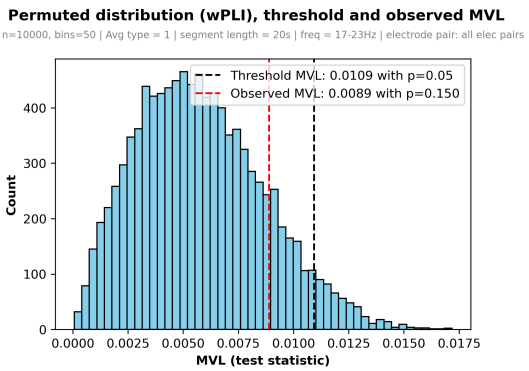

(B) Permuted distribution for ImCoh with the observed MVL correlating to p=0.150.

FIGURE 22: Permuted distributions for ImCoh and wPLI of the test statistic MVL (n=10000, visualized with 50 bins) with a black dashed line representing the threshold MVL (p=0.05) and the dashed red line representing the observed MVL. Base settings were used.

Effect of tACS over several time windows

In these figures, we extend our analysis beyond the initial segment of the post-stimulation block. Beginning with the initial segment, we use a 20-second window (from base settings) that is successively shifted by 5-second increments until reaching the final segment from 40 to 60 seconds. This approach allows us to observe temporal variations in the change of FC during the first minute after stimulation. Each figure presents the results for each of the four phase lag conditions in comparison to the sham condition. We illustrate the variance by displaying the ±1 standard deviation for each segment. The comparison for AP vs SH is demonstrated in Figure 23 for both ImCoh and wPLI, as this comparison showed the greatest difference between a phase lag condition and SH. Some differences in the mean are observed during the first three time windows (up to 10-30 seconds). After these time windows, this difference disappears.

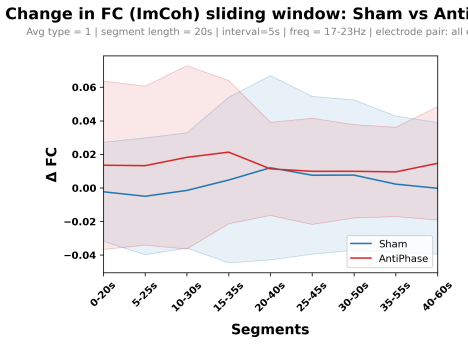

(A) ΔImCoh: AP vs SH.

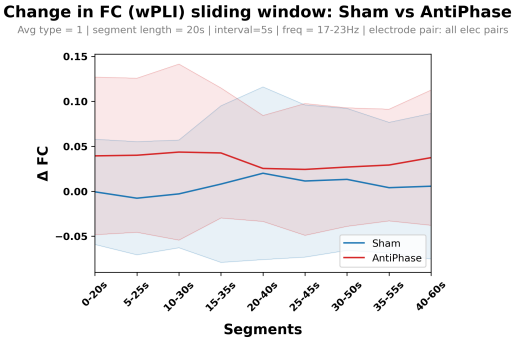

(B) ΔwPLI: AP vs SH.

FIGURE 23: Comparison of FC changes over 20s time windows (slid every 5s) between different conditions for the full one minute after stimulation. Each line represents the average FC value for the respective condition, with the shaded region indicating the range of variability represented by ± standard deviations. The x-axis denotes the time intervals after stimulation onset, ranging from 0 to 60 seconds in 5-second increments, and the y-axis denotes the change in FC for each of these time intervals. Base settings were used.

3.2 Optimization of settings

All other parameter configurations have undergone testing. For conciseness, we exclusively present the p-values for ImCoh and wPLI after permutation statistics in Table 3.

Parameter setting	**ImCoh**	**wPLI**
Base	p=0.360	p=0.150
Elec. pair CCP5h-CCP6h	p=0.827	p=0.596
Elec. pair FFC5h-FFC6h	p=0.627	p=0.740
Elec. pair FCC3h-FCC4h	p=0.136	p=0.043*
Elec. pair CCP3h-CCP4h	p=0.986	p=0.765
Elec. pair C5-C6	p=0.285	p=0.076
Frequency band 13-30 Hz	p=0.366	p=0.096
Frequency band 15-25 Hz	p=0.224	p=0.059
Frequency band 19-21 Hz	p=0.703	p=0.462
Epoch length 12s	p=0.900	p=0.625
Epoch length 30s	p=0.560	p=0.477
Averaging type 0	p=0.185	p=0.155
Averaging type 2	p=0.302	p=0.228

TABLE 3: P-values for both ImCoh and weighted Phase Lag Index wPLI across different experimental settings. The first row presents p-values for base settings, indicating the statistical significance of ImCoh and wPLI. Subsequent rows represent variations from base settings, with corresponding p-values for both ImCoh and wPLI, demonstrating the impact of parameter modifications on the FC measurements. *Significant non-uniform distribution for $p<0.05$.

The current analysis has revealed a statistically significant non-uniform distribution across phase lags for the electrode pair FCC3h-FCC4h. However, following multiple comparisons tests, none of the corrected p-values reached significance.

Upon further investigation, electrode pair C5-C6 exhibited a relatively low p-value (p=0.076). Moreover, frequency bands spanning 13-30 Hz (p=0.096) and 15-25 Hz (p=0.059) demonstrated trends toward significance in comparison to narrower bandwidths. Consequently, it was proposed to leverage this information by optimizing these parameters to focus on electrode pairs of interest (FCC3h-FCC4h, C5-C6) in conjunction with a broader frequency band (13-30 Hz). In addition, adjacent electrode pairs in proximity to FCC3h-FCC4h and C5-C6 were explored.

The p-values after permutation statistics for these optimized parameter settings are demonstrated in Table 4.

Electrode pair	**ImCoh**	**wPLI**
CCP5h-CCP6h	p=0.615	p=0.329
FFC5h-FFC6h	p=0.667	p=0.556
FCC3h-FCC4h	p=0.360	p=0.080
CCP3h-CCP4h	p=0.575	p=0.891
C5-C6	p=0.178	p=0.034*
FC1-FC2	p=0.800	p=0.564
FC5-FC6	p=0.289	p=0.032*
FT7-FT8	p=0.849	p=0.873
T7-T8	p=0.466	p=0.175

TABLE 4: Statistical examination of both previously examined and additional electrode pairs was conducted using permutation statistics of the MVL. The resulting p-values are presented for both ImCoh and wPLI. The analysis encompasses the full beta frequency band ranging from 13 to 30 Hz. *Significant non-uniform distribution for $p<0.05$.

For the full beta-band, the electrode pair C5-C6 becomes significant (from p=0.076 to p=0.032), whereas the electrode pair FCC3h-FCC4h no longer retains significance (from p=0.043 to p=0.080), albeit remaining relatively proximate to significance. Among the additional electrode pairs, it was found that FC5-FC6 exhibits significance (p=0.032). Figure 14 was subsequently updated by highlighting electrode pairs demonstrating significance within specific frequency bands (17-23 Hz or 13-30 Hz) in green, while those lacking significance were highlighted in red. The updated figure is presented as Figure 24.

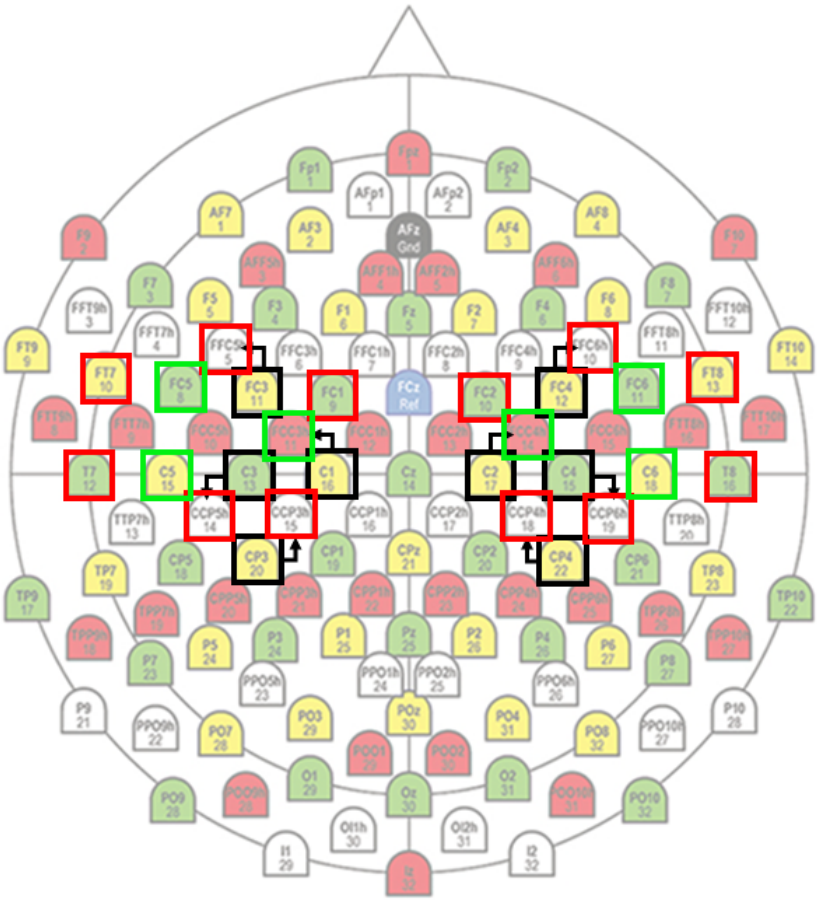

FIGURE 24: Visualization of the 10-10 electrode system with all tested electrode pairs highlighted, figure taken from Brain Products GmbH [44]. Green denotes electrode pairs exhibiting significance within the beta-band (17-23 Hz or 13-30 Hz), while red indicates electrode pairs where significance within the beta-band was not observed.

To assess the impact of varying the width of the frequency band on the uniformity of ΔFC across phase lags, supplementary tests were performed using the optimized selection of electrode pairs. Results are published in Table 5.

Frequency band	ImCoh	wPLI
13-30 Hz	p=0.187	p=0.016*
15-25 Hz	p=0.021*	p=0.001*
17-23 Hz	p=0.010*	p=0.001*
19-21 Hz	p=0.048*	p=0.022*

TABLE 5: Statistical examination of the frequency band for optimal electrode pair selection was conducted using permutation statistics of the MVL. The resulting p-values are presented for both ImCoh and wPLI. The analysis encompasses the full beta frequency band ranging from 13 to 30 Hz. *Significant non-uniform distribution for $p<0.05$.

Similarly, to assess the impact of varying the epoch length, supplementary tests were performed using the optimized selection of electrode pairs. Results are published in Table 6.

Epoch length	ImCoh	wPLI
12s	p=0.919	p=0.396
20s	p=0.187	p=0.016*
30s	p=0.357	p=0.094

TABLE 6: Statistical examination of the epoch length (in seconds) for optimal electrode pair selection was conducted using permutation statistics of the MVL. The resulting p-values are presented for both ImCoh and wPLI. Analysis encompasses the full beta frequency band ranging from 13 to 30 Hz. *Significant non-uniform distribution for $p<0.05$.

Finally, to assess the impact of the averaging type used, regarding the inclusion or exclusion of post-stimulation blocks, supplementary tests were performed using the optimized selection of electrode pairs. Results are published in Table 7.

Averaging type	ImCoh	wPLI
Type 0	p=0.090	p=0.071
Type 1	p=0.187	p=0.016*
Type 2	p=0.232	p=0.075

TABLE 7: Statistical examination of the averaging type for optimal electrode pair selection was conducted using permutation statistics of the MVL. The resulting p-values are presented for both ImCoh and wPLI. The analysis encompasses the full beta frequency band ranging from 13 to 30 Hz. *Significant non-uniform distribution for $p<0.05$.

After optimization of the parameter settings, it was observed that:

- Electrode pairs: In addition to the significant electrode pair FCC3h-FCC4h, we found for C5-C6 a relatively low p-value of 0.076 for wPLI. Other electrode pairs used for EEG measurement were investigated adjacent to these electrode pairs (FCC3h-FCC4h, C5-C6) for relatively low p-values ($p<0.10$). This led to our finding that FC5-FC6 also showed a significant result for 17-23 Hz (wPLI: $p<0.0001$). Besides, it is worth noting that this was the only instance where significance for ImCoh was observed ($p=0.002$).
- Frequency band: Broader frequency bands exhibited p-values below 0.10, specifically, the 15-25 Hz band ($p=0.059$) and the 13-30 Hz band ($p=0.076$);
- Averaging type: The p-values exhibited little variation, which justifies retaining the averaging type that incorporates all data (averaging type 1);
- Epoch length: A substantial increase in the p-value was observed upon either decreasing (12s) or increasing (30s) the epoch length, thus indicating to maintain an epoch length of 20s.

In our final results, we selected a combination of electrode pairs that demonstrated p-values lower than 0.10 within the 13-30 Hz frequency range: FCC3h-FCC4h, C5-C6, and FC5-FC6.

3.3 Final results with optimal settings

When averaging over the selected electrode pairs within the full beta-band (13-30 Hz), we observed a p-value of p=0.189 for ImCoh and a p-value of p=0.017 for wPLI. We further investigate the significant results for wPLI within Figures 25, 26, 27 and 28.

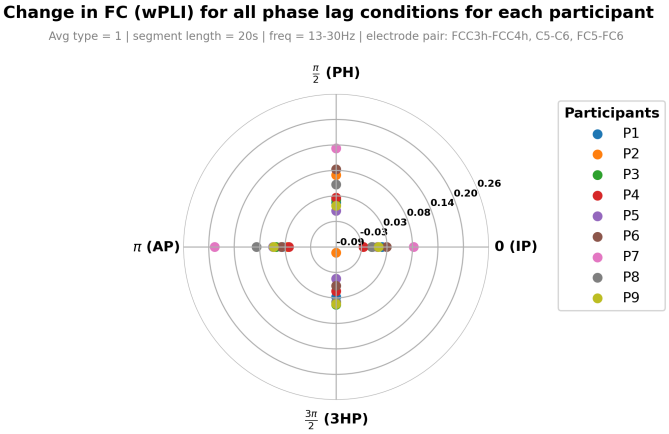

FIGURE 25: Average ΔFC measured by wPLI for all phase lag conditions for each participant. ΔFC values range from approximately -0.09 (origin of the polar plot) to 0.26 (outer radius of the polar plot). Optimized electrode pairs, full beta-band settings.

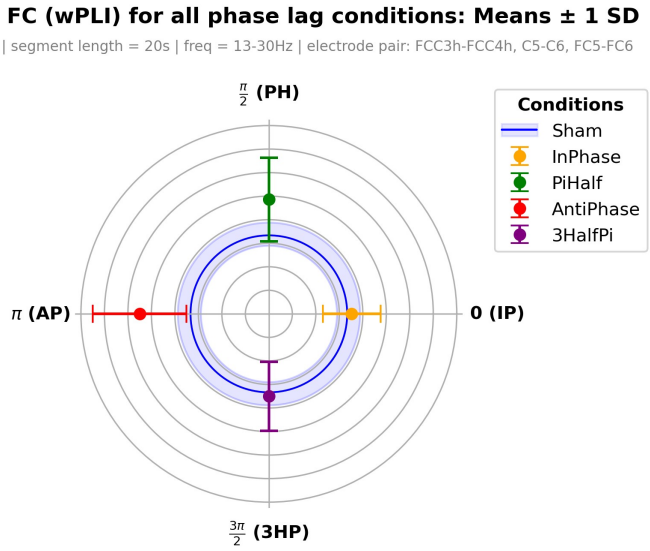

FIGURE 26: Change in FC (wPLI) for all phase lag conditions: means ±1 standard deviation (SD). Here it is observed that the means for AP and PH extend beyond the +1 SD ring of the sham condition, while the means for IP and 3HP align closely with the mean of the sham condition. Optimized electrode pairs, full beta-band settings were used.

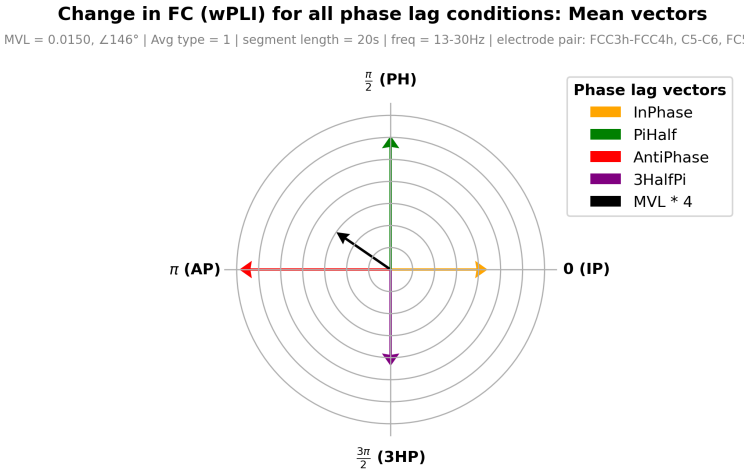

FIGURE 27: Comparison of changes in FC across various phase lag conditions using ImCoh and wPLI measures. Each colored vector represents the mean of a specific phase lag condition. The black vector represents the MVL, enlarged by a factor of 4 for illustrative purposes. The length (0.0150) and phase angle (146°) of the MVL are depicted in the grey subtitle, along with the optimized electrode pairs and full beta-band settings.

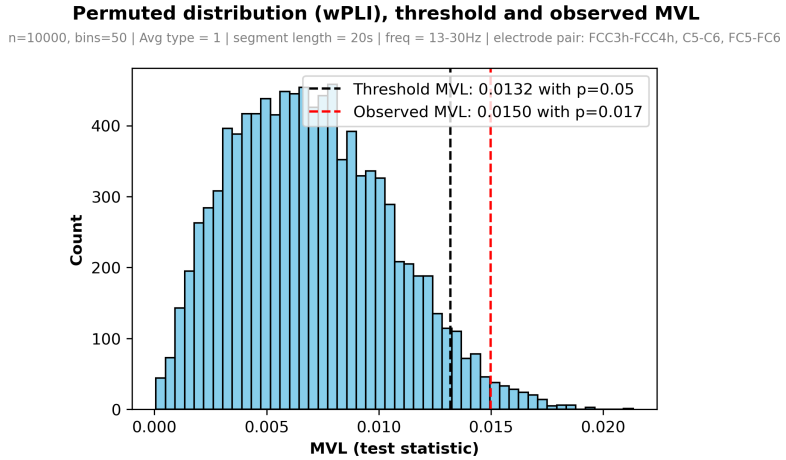

FIGURE 28: Permuted distribution (wPLI) of the test statistic MVL (n=10000, visualized with 50 bins), the threshold MVL (p=0.05) and the observed MVL (p=0.017). Optimized electrode pairs, full beta-band settings.

All condition comparisons have been investigated, with their corresponding p-values documented in Table 8.

Comparison	Non-adjusted p-value	Adjusted p-value
SH-IP	0.734	1.000
SH-PH	0.039	0.391
SH-AP	0.004	0.039*
SH-3HP	0.800	1.000
IP-PH	0.014	0.144
IP-AP	0.002	0.022*
IP-3HP	0.966	1.000
PH-AP	0.300	1.000
PH-3HP	0.151	1.000
AP-3HP	0.017	0.174

TABLE 8: Summary of multiple comparisons tests for comparisons between all (ten) conditions. Non-adjusted and adjusted p-values by Bonferroni-correction are demonstrated. *Indicates a significant difference in ΔFC between conditions after correction ($p<0.05$).

Hence, significant differences in ΔFC were observed between the SH-AP and IP-AP conditions. We further investigated the temporal variations over the entire minute for these conditions in Figure 29 for both significant comparisons.

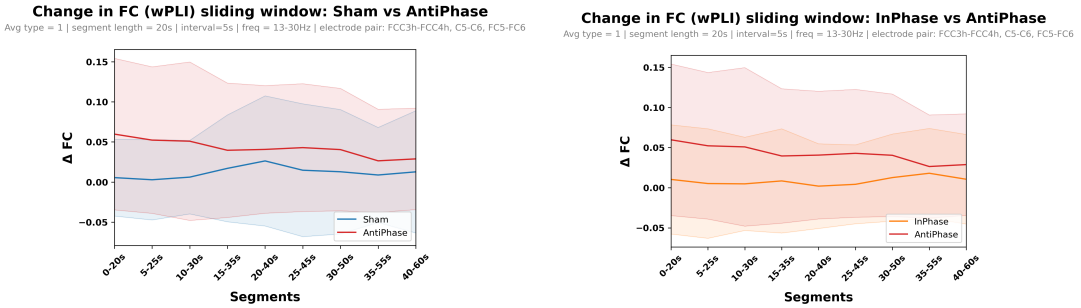

(A) ΔwPLI: AntiPhase vs Sham.

(B) ΔwPLI: InPhase vs AntiPhase.

FIGURE 29: Comparison of FC changes over 20s time windows (slid every 5s) between different conditions for the full 1 minute after stimulation. Each line represents the average FC value for the respective condition, with the shaded region indicating the range of variability represented by ±1 standard deviations. The x-axis denotes the time intervals after stimulation onset, ranging from 0 to 60 seconds in 5-second increments, and the y-axis denotes the change in FC for each of these time intervals. Optimized electrode pairs, full beta-band settings were used.

Furthermore, in response to the unexpected increase in p-value observed with an epoch length of 12s (compared to 20s), an added examination of temporal dynamics was undertaken. Specifically, temporal variation was investigated using epochs of 12s with incremental steps of 3s, optimized electrode selection, and a more narrow frequency band (17-23 Hz) was selected for further analysis.

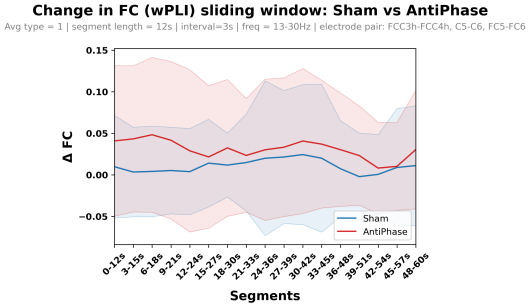

(A) ΔwPLI: AntiPhase vs Sham.

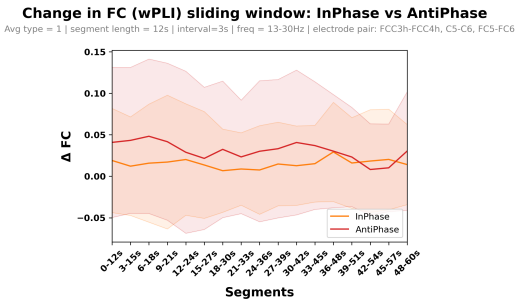

(B) ΔwPLI: InPhase vs AntiPhase.

FIGURE 30: Comparison of FC changes over 12s time windows (slid every 3s) between different conditions for the full 1 minute after stimulation. Each line represents the average FC value for the respective condition, with the shaded region indicating the range of variability represented by ±1 standard deviations. The x-axis denotes the time intervals after stimulation onset, ranging from 0 to 60 seconds in 3-second increments, and the y-axis denotes the change in FC for each of these time intervals. Optimized electrode pairs, full beta-band settings were used.

4 Discussion

4.1 Key findings

In this study, our primary objective was to investigate how the phase lag condition in dual-site HD-tACS modulates beta-band FC between the M1s through the analysis of resting-state EEG. We hypothesized that different phase lag conditions would result in varying changes in FC, as we found variable outcomes in preceding research [9–15, 29]. Our analysis of FC changes (ΔFC) across four phase lag conditions (IP, PH, AP, and 3HP) and a sham condition (SH) revealed a significant difference between the SH-AP and IP-AP conditions, as shown in Table 8. A circular visualization of these conditions, presented in Figure 26, indicates a significant increase in FC for the AP condition compared to both SH and IP.

A secondary objective was to research which FC measure effectively captures the observed changes in FC. We hypothesized similar outcomes as the main difference between the two measures is the inclusion/exclusion of amplitude and similar power (= amplitude^2) throughout the measurements was expected. Our research suggests that wPLI captures changes in FC better than ImCoh does.

Another secondary objective of this study was to identify parameter settings (electrode pair selection, frequency band, epoch length, and averaging type) that effectively capture the observed changes in FC. Our results indicated that for our specific dual-site HD-tACS 3-to-1 montage setup, the electrode pairs FCC3h-FCC4h, C5-C6, and FC5-FC6 were effective. For future studies with a similar setup, the electrode pair FCC5h-FCC6h is recommended over the FFC5h-FFC6h pair used in this study. Although the more conventional 13-30 Hz frequency band was used for our final results, our findings suggest that a more narrow band of 17-23 Hz more effectively captures changes in FC. Regarding epoch length, an epoch of 20 seconds is advisable. For averaging type, averaging over all post-stimulation data blocks (type 1) is recommended.

4.2 Change in FC for varied phase lags

Our findings combined with previous studies [9–15, 29] suggest that the phase lag condition is an important factor, but it is still unpredictable whether a specific phase lag causes an increase or decrease in FC, in case any change in FC was measured to begin with. In a field with dual-site tACS studies investigating phase lag conditions by measuring FC, we can compare our findings with those presented earlier in Table 1, which includes eight studies [9–15, 29]. In these studies, we observed an increased FC for IP compared to AP in the studies conducted by Meng et al., Schwab et al., Helfrich et al., and Polanía et al. [9, 12, 14, 15]. However, the other four studies reported either an increase in FC for AP or no change at all. Combined with our findings, which indicate a relative increase for AP, there is no consistent outcome for FC modulation based on a specific phase lag.

As we have attempted to compare with previous studies from a global standpoint, to our knowledge, no prior studies have investigated the impact of the phase lag within dual-site tACS on FC under similar conditions. These conditions include the electrode montage (3-to-1 HD), the location of stimulation (bilateral M1 regions), and the state of the participant while measuring EEG (resting-state). Each of these factors can contribute to varying outcomes across studies. For instance, we can attempt a comparison with beta-band studies in particular from Meng et al. and Tan et al. [12, 13]. Both studies explored resting-state EEG under IP and AP conditions within a broad beta-band range (13-30 Hz, 14-33 Hz), with a 20 Hz stimulus applied to two regions. However, the locations of stimulation differ not only in location but also in proximity, with the two stimulation sites being relatively nearby.

In contrast, our study focuses on long-range interhemispheric connectivity, i.e., connectivity between distant regions in which each region is located in a different hemisphere. This way, a better comparison could perhaps be made with other interhemispheric FC studies, such as from Schwab et al., Helfrich et al., and Strüber et al. [10, 14, 15]. However, these studies analyzed a different frequency band. Regardless of how we examine these studies combined with our results, the conclusion remains that when considering IP, AP, and SH conditions, it remains hard to predict what type of change a specific phase lag will cause if any change in FC is measured.

In addition, we have considered two additional phase lag conditions that have not been previously examined in any dual-site tACS study: PH and 3HP. Our results suggest a trend indicating that PH may increase FC compared to SH and 3HP. This is supported by the results shown in Figures 26 and 27, where the mean FC for PH extends beyond the ±1 SD sham region in Figure 26, unlike 3HP. Furthermore, the phase preference of the MVL observed in Figure 27 aligns not only in the direction of AP (180 degrees) but also in the direction of PH (90 degrees), as indicated by the MVL angle of 146 degrees. However, these differences did not reach statistical significance. Despite the lack of statistical significance, the observed trend warrants further investigation to better understand the effects of these phase lags and their role within the broader context of all phase lags.

4.3 FC measure comparison: ImCoh and wPLI

When testing for a non-uniform distribution across the phase lag conditions, we consistently observed lower p-values for wPLI compared to ImCoh, when considering p-values < 0.5 (see Tables 3, 4, 5, 6, and 7). Notably, this difference becomes important when considering our final results, where we used a frequency band of 13-30 Hz (further explanation of this choice in 4.4.2). When we assessed various frequency bands (see Table 5), we observe that a significant non-uniform distribution was identified for both ImCoh and wPLI when averaging over the optimized electrode pairs and utilizing beta-bands of 15-25 Hz, 17-23 Hz, and 19-21 Hz. However, when using the full 13-30 Hz beta-band, significance was retained only for wPLI (p=0.016), while ImCoh remained relatively far from significance (p=0.187).

This phenomenon, where significant results are found for wPLI but not for ImCoh, was observed in our analysis of other parameters as well. When assessing individual electrode pairs (see 3), a significant ΔFC was found for the electrode pair FCC3h-FCC4h using wPLI, but not with ImCoh. When evaluating epoch length, specifically an epoch length of 20 seconds, we observed a significant p-value for wPLI, whereas ImCoh did not yield a significant result. Lastly, when examining the averaging type, a significant ΔFC was identified for averaging type 1 using wPLI, but not while using ImCoh (see 7). This prompts the question of whether the observed significant ΔFC for wPLI is spurious, or if ImCoh is overly constrictive in filtering out FC.

To make a fair comparison, it is crucial to re-examine the computational differences between these measures closely. The primary distinction is the inclusion or exclusion of amplitude in the calculation. As noted in the introduction (see 1.4.5), Nolte et al. contend that considering amplitude is imperative, as low amplitude signals are considered weak and therefore easily disturbed by noise [40]. Hence, weighing down low amplitude signals provides higher reliability in the measurement of the phase component. Therefore, Nolte et al. advocate using ImCoh to measure FC. Nonetheless, it is plausible that this hypothesis may not hold. By giving less significance to measurements with lower amplitude, there is a risk of discarding data that could offer equally explanatory phase measurements, leading to an excessively conservative measure. To tackle this potential problem, Stam et al. proposed the PLI [39], which gives equal weight to signals of all amplitudes. Later, Vinck et al. proposed using wPLI to retain the favorable properties of ImCoh, which is robustness against spurious FC at a 0/pi phase-lag caused by volume conduction [38]. In addition to considering the computational properties of ImCoh and wPLI, we must address our assumption that all signals have equal power throughout the measurement. This assumption is likely violated to some extent. Because if the power were entirely equal, the results of these significance tests would be very similar. In another ongoing study within our research group, this power is under investigation to verify that we have similar power throughout the measurement.

Considering the equal power assumption, our hypothesis of expecting changes in FC, and the result of finding more significant changes in FC with wPLI compared to ImCoh, we cautiously conclude that wPLI best captures ΔFC. These observations suggest that ImCoh may be too conservative in measuring FC by eliminating weak signal data that might contain true FC. However, we must be cautious in making this claim, as from an experimental standpoint alone, it is impossible to determine whether the low amplitude signals represent true FC or spurious FC. Nevertheless, we can further investigate the power dynamics in our experiment, which is being addressed in our parallel ongoing study. If the power does not significantly change throughout the experiment, it

would indicate that relatively low amplitude signals do not differ significantly from relatively high amplitude signals. Consequently, weakening the impact of relatively low amplitude signals would be less justified, as they could contain valuable data. This would provide a stronger foundation for our recommendation to use wPLI over ImCoh.

4.4 Parameter settings

To achieve the final results in our study (see 3.3), we initially tested our preliminary findings using pre-determined base settings. After finding no significant ΔFC with these base settings (see 3.1), we proceeded to analyze each setting within the four parameters: averaging type, epoch length, frequency band, and electrode pairs. As described in the Methods section (see 2.10), we examined the p-values to identify significance ($p<0.05$) and near-significance ($p<0.10$) as shown in Table 3. Through this detailed analysis, we determined that changing one parameter — the selection of electrode pairs — was necessary. For our final results, we used an optimized set of electrode pairs (FCC3h-FCC4h, C5-C6, and FC5-FC6). Additionally, we adjusted the frequency band to the more conventional 13-30 Hz for better comparison with other beta-band studies. The settings of other parameters remained the same, specifically, we retained averaging type 1 and an epoch length of 20 seconds. Further elaboration on these choices is provided in the following paragraphs.

4.4.1 Electrode pairs

The adjustment of electrode pair selection was based on statistical tests for each pair, as presented in Table 4. We focused here in wPLI, based on our findings as discussed in section 4.3. We hypothesized that with the electrode pairs used in base settings (CCP5h-CCP6h, FCC5h-FCC6h, FCC3h-FCC4h, CCP3h-CCP4h, and C5-C6), which are placed close to the stimulation site, would be able to capture changes in FC. However, we did not find a significant result when averaging over these five electrode pairs, as earlier discussed in our Methods section (24). Taking a closer look at the individual electrode pairs in Table 3, we found that electrode pairs CCP5h-CCP6h, FFC5h-FFC6h, and CCP3h-CCP4h exhibited p-values exceeding 0.3, suggesting an absence of significant modulation in FC by tACS. Besides, we did find for electrode pair FCC3h-FCC4h a significant result ($p=0.043$) and for C5-C6 a near significant p-value ($p=0.076$).

To optimize our electrode pair selection, we expanded our analysis to include additional pairs surrounding the pairs from base settings (FCC3h-FCC4h and C5-C6) that demonstrated potential for capturing changes in FC. Figure 24 visualizes the electrode pairs selected for further analysis (in green) and those discarded (in red). All green pairs exhibited significance for some beta-band: FC5-FC6 (13-30 Hz), C5-C6 (13-30 Hz), and FCC3h-FCC4h (17-23 Hz). For the beta-band used in our final results (13-30 Hz), each selected pair had p-values below 0.10. This threshold was chosen to maximize the inclusion of electrode pairs, thereby increasing data volume and enhancing the likelihood of achieving collective significance. Notably, FCC3h-FCC4h was significant for the 17-23 Hz band and near significant for the 13-30 Hz band ($p=0.08$). Excluding this pair from the final selection was deemed unfavorable due to its strong potential for contributing valuable data and improving the overall significance of the multi-electrode pair selection.

Upon revisiting Figure 24, it becomes apparent that the electrode pair FCC5h-FCC6h should be included in future experiment designs using the same electrode montage. This figure shows that FCC5h-FCC6h is surrounded by other green-marked electrode pairs demonstrating significant results. Therefore, rather than substituting the stimulation electrode pair FC3-FC4 with FFC5h-FCC6h (a non-significant electrode pair from the base settings), it appears more logical to incorporate FCC5h-FCC6h instead.

Including electrode pair FCC5h-FCC6h could have potentially enhanced the statistical power of our analysis. We cannot change the set-up for our ongoing study, but in future study designs, incorporating this electrode could validate whether the optimal electrode selection for assessing the effects of dual-site tACS on the M1 with our chosen 3-to-1 montage indeed comprises a combination of FCC3h-FCC4h, FC5-FC6, C5-C6, and FCC5h-FCC6h.

In addition, this finding underscores that when employing electrical stimulation and EEG mea-

surements, the anticipated effects may manifest in locations slightly different from the initial assumptions. In our case, the found effect was more frontal and lateral than expected. Therefore, we recommend a broader spatial exploration of the region surrounding the stimulation electrodes.

In addition, in future investigations, it would be valuable to validate the precise stimulation locations through simulations. Specifically, it would be intriguing to ascertain whether electrodes FCC3h-FCC4h, FC5-FC6, C5-C6, and FCC5h-FCC6h indeed exhibit optimal sensitivity to the effects induced by our chosen dual-site tACS electrode montage. If these electrodes prove to be the most effective in capturing the desired effects, simulations could help forecast which additional electrodes, beyond the standard 64-measurement 10-10 electrode configuration, should replace the stimulation electrodes. This would prevent the loss of valuable data, as demonstrated with FCC5h-FCC6h. Overall, such simulations hold promise in predicting the electrodes that would most effectively capture the modulations in brain activity across any chosen electrode montage.

4.4.2 Frequency band

It was unknown to what extent the effect of tACS would remain notable when including frequencies further away from the stimulation frequency (20 Hz). The effect might fade away when including frequencies near the edges of the full beta-band. On the other hand, taking a very narrow frequency band is also undesirable, as there may not be enough signal power to reliably detect changes in FC, leading to a lower signal-to-noise ratio.

Based on the p-values from Table 5, the most favorable frequency bands appear to be within 15-25 Hz or 17-23 Hz. These bands exhibit relatively lower p-values for ImCoh and wPLI when relating to narrower (19-21 Hz) and broader (13-30 Hz) frequency bands. Given our results, by selecting a bandwidth of only 2 Hz, we might have missed modulation effects beyond the band of 19-21 Hz. Additionally, frequency bands broader than 15-25 Hz may include data no longer affected by tACS.

However, caution is warranted when interpreting these results based solely on p-values. While p-values inform us about the reliability of the observed change in FC being attributable to tACS, they do not convey the magnitude of this effect. Given that all tested frequency bands for the optimal electrode pairs exhibited statistical significance, assessing the effect size is crucial to fully comprehend the impact of tACS on FC across various frequency bands. Therefore, future studies should include effect size analysis.

In an extended frequency band analysis, it is also beneficial to investigate individual discrete frequencies rather than averaging them directly. This approach involves generating an intermediate plot of discrete frequencies before averaging, allowing for a more detailed examination of how the 20 Hz stimulus affects surrounding frequencies. By doing this, we can gain a clearer understanding of the specific frequency response to tACS. Currently, we assume the highest effect to be around 20 Hz, with the effect diminishing at frequencies further from the stimulation frequency, but this has not been conclusively demonstrated. Finding relatively higher p-values for the 19-21 Hz band encourages this extended frequency band analysis. For the final analysis in this study, we chose to use the broadest frequency band of 13-30 Hz. This decision facilitates comparability with other dual-site tACS studies focusing on beta-band activity [12, 13].

4.4.3 Epoch length and temporal dynamics

The base setting of using a 20s epoch length appeared appropriate for this study. Both shorter (12s) and longer epoch lengths (30s) yielded non-significant results, contrasting with the significant findings observed with the 20s epoch length. The increase in p-value with a larger epoch length, leading to loss of significance, can be explained by potential decay in the effect of tACS after $\pm$ 20s. For a shorter epoch length, we also find an increase in p-value accompanied by a loss of significance. This result is somewhat unexpected, as the effect of tACS is likely to be strong immediately after stimulation.

One plausible explanation for this phenomenon could be that the initial seconds ($<$12s) of the recording did not capture the tACS effect, while the subsequent seconds up to 20s did capture the

effect. As we cannot reliably investigate epoch lengths shorter than 12s [49], we delved deeper into this phenomenon by examining the temporal dynamics using a sliding window figure, illustrated in Figure 30. We ensured the utilization of the optimized electrode pairs. We hypothesized the possibility of observing an increased difference within the SH-AP or IP-AP comparisons in later time windows (with 3s shifts) following the initial 12s, such as the 9-21s interval. Although the sliding window figures are not statistically tested, it appears that there is no increase for both AP-SH and IP-SH during the 9-21s interval.

The most plausible explanation for not finding a significant result for a shorter epoch length of 12s is the lack of data. When inspecting Figure **??**, we observe some changes in FC for the 0-12s and 3-15s time windows. However, at least for the 0-12s window, the observed ΔFC was not significant but could become significant with a larger dataset. In general, analyzing a larger group of participants will help clarify why a 20s epoch length was the most suitable for our study. Moreover, we recommend adding a statistical assessment for all epoch lengths too. This extended research would be valuable, given that the epoch length appears to have a substantial impact on the results and there is limited coverage in the literature [49–51].

4.4.4 Averaging type

The primary objective of assessing the averaging type was to determine whether including the first post-stimulation block, immediately following the longest stimulation period of 5 minutes, yielded different results compared to the subsequent post-stimulation blocks, which followed 1-minute stimulations. To assess this, we used three different averaging types: averaging type 0, which included only the first post-stimulation block following a 5-minute stimulation; averaging type 1, which included all six post-stimulation blocks; and averaging type 2, which included only the last five post-stimulation blocks following 1-minute stimulations.

Averaging type 1 emerged as the sole statistically significant (wPLI) averaging type when using the optimal electrode pair selection, as shown in Table 7. Including only the first post-stimulation block after the longest stimulation period of 5 minutes, allows us to test whether a longer continuous stimulation period is necessary to observe an effect or if inclusion of the subsequent 1-minute blocks is required to ensure more robust data. Our results support the latter. That is, the additional blocks seems to help mitigate the influence of outliers and improve the signal-to-noise ratio.

One limitation of our study is the decision to equalize the number of pre- and post-stimulation segments, particularly affecting averaging type 0. We decided to equalize the number of post-stimulation segments with the number of pre-stimulation segments, even when more pre-stimulation segments were available. For instance, with averaging type 1 and an epoch length of 20 seconds, we used six stimulation segments but could have included nine 20s pre-stimulation segments from the full 3-minute pre-stimulation block. This was done to ensure a fair comparison between the averaged post-stimulation and pre-stimulation blocks by using the same number of segments. However, this approach results in the exclusion of some pre-stimulation data, potentially reducing the reliability of the averaged pre-stimulation FC data. This issue is particularly pronounced when assessing averaging type 0, where we have only one post-stimulation segment. The inability to average multiple segments becomes apparent for both post- and pre-stimulation data. This issue could have been avoided by including as many pre-stimulation segments as possible to average over (e.g. nine segments, when using a 20s epoch length). In conclusion, the results for averaging type 0 seem very unreliable, suggesting that the analysis of averaging methods should have been approached differently or excluded altogether.

We used averaging type 2 to assess the influence of the first post-stimulation block and found it to play a crucial role in finding a significant change in FC. Indirectly, by excluding the first block, averaging type 2 allows us to evaluate the potential effect, or lack thereof, of the longer 5-minute stimulation period. For averaging type 2, we still have five segments to average over, which was considered to be a sufficient number to maintain robust data. However, the p-value rises for averaging type 2 compared to averaging type 1, accompanied by a loss of significance. This suggests that the initial post-stimulation block holds substantial importance in our dataset.

4.5 Future work

A primary limitation of this study is the small sample size of only nine participants, which inherently reduces the statistical power and reliability of our conclusions. In Section 4.4.3, we have highlighted a situation where this limitation may have played a role in finding significance for within a 0-20s interval but not for 0-12s. However, this limitation is currently being addressed, as the study is ongoing and aims to include a total of 30 participants in the near future.

EEG recordings obtained from the scalp offer valuable insights into brain activity, yet they come with inherent limitations, like volume conduction [34]. There are two methods that can be used to allow for more accurate analysis of electrophysiological signals: source reconstruction and spatial filtering.

Source reconstruction involves a mathematical technique that enables the estimation of the specific brain regions generating the recorded EEG signals. By pinpointing the origins of brain activity, source reconstruction enhances the precision of analysis, while minimizing the influence of volume conduction and other artifacts or sources of noise [34].

By implementing spatial filtering, it becomes feasible to detect true 0 and π phase-lag connectivity, addressing a significant limitation of the lagged connectivity methods used in our study. In addressing volume conduction in EEG data analysis, two primary approaches are commonly employed: spatial filtering and lagged connectivity methods [34]. While our project focused on investigating lagged connectivity methods, particularly wPLI, spatial filtering techniques offer an effective alternative. Methods such as the surface Laplacian [13] are applied directly to the sensor-level EEG data and are suitable for setups with at least 64 electrodes [34]. Unlike lagged connectivity methods, spatial filtering can effectively address volume conduction and reveal true phase-lag connectivity.

While source reconstruction and spatial filtering are distinct methods, they are often used together [13, 58]. Spatial filtering can be used as a preprocessing step to enhance signal quality before applying source reconstruction. Both methods aim to improve the accuracy of EEG analysis but operate at different stages of the data processing pipeline. Source reconstruction typically follows spatial filtering to further localize brain activity with reduced artifacts.

Overall, combining spatial filtering, source reconstruction and an increased sample size can help us validate our main conclusions regarding the significant changes in FC for SH-AP and IP-AP. Additionally, they can provide insights into why these significant changes are observed when measuring from electrode pairs FC5-FC6, C5-C6, and FCC3h-FCC4h. Furthermore, this approach can verify our claim that wPLI better captures changes in FC than ImCoh. Lastly, with these two methods we can further investigate our findings regarding the parameter settings, the frequency band in particular. That is, we can then enhance our understanding of which beta frequency band is most appropriate for assessing the effects of a 20 Hz stimulation frequency.

5 Conclusion

In this study, we have demonstrated a significant change in FC after applying dual-site beta-tACS on both M1s between the conditions SH-AP and IP-AP. AP demonstrated a significant increase in FC compared to SH and IP. As this is not a common result in other studies investigating the role of the phase lag in dual-site tACS, this study highlights the variability in outcomes, emphasizing the need for further investigation of the phase lag. Besides, our study assessed two commonly used FC measures: ImCoh and wPLI. We found that wPLI commonly identified significant results where ImCoh did not, suggesting that wPLI is a more reliable measure of FC. Furthermore, we have assessed various parameters in our study design. Most notably, we found a different set of electrode pairs than initially expected that captures changes in FC best and recommended one additional electrode pair to add in future research with the same HD electrode montage. Future work holds an expansion of the sample size from nine to 30 participants, which will increase our study's statistical power and reliability of our findings. Additionally, the combination of spatial filtering and source reconstruction is recommended for a more accurate analysis of electrophysiological signals.

Contributions

Brighton Z. de Jong, BSc: Drafted thesis report, conducted functional connectivity analysis, provided assistance with the preprocessing pipeline. **ir. Silvana Huertas Penen**: Provided primary supervision, led the dual-site tACS experiments, experimental design, oversaw and ultimately performed preprocessing procedures, reviewed the report. **dr.ir. Bettina C. Schwab**: Provided secondary supervision, experimental design, project lead, reviewed the report. **dr.rer.nat. Maria Carla Piastra**: Reviewed the report. **Thomas van Genderen, BSc**: Provided assistance with the preprocessing pipeline, provided assistance with the dual-site tACS experiments.

References

1. Del Felice, A. *et al.* Personalized transcranial alternating current stimulation (tACS) and physical therapy to treat motor and cognitive symptoms in Parkinson's disease: A randomized cross-over trial. *NeuroImage: Clinical* **22,** 101768. ISSN: 2213-1582 (Jan. 2019).
2. Benussi, A. *et al.* Increasing Brain Gamma Activity Improves Episodic Memory and Restores Cholinergic Dysfunction in Alzheimer's Disease. *Annals of Neurology* **92,** 322–334. eprint: https://onlinelibrary.wiley.com/doi/pdf/10.1002/ana.26411. https://onlinelibrary.wiley.com/doi/abs/10.1002/ana.26411 (2022).
3. Alexander, M. L. *et al.* Double-blind, randomized pilot clinical trial targeting alpha oscillations with transcranial alternating current stimulation (tACS) for the treatment of major depressive disorder (MDD). *Translational Psychiatry* **9,** 106. https://doi.org/10.1038/s41398-019-0439-0 (2019).
4. Ahn, S. *et al.* Targeting reduced neural oscillations in patients with schizophrenia by transcranial alternating current stimulation. *NeuroImage* **186,** 126–136. ISSN: 1053-8119. https://www.sciencedirect.com/science/article/pii/S1053811918320287 (2019).
5. Wischnewski, M., Alekseichuk, I. & Opitz, A. Neurocognitive, Physiological, and Biophysical Effects of Transcranial Alternating Current Stimulation. *Trends in Cognitive Sciences* **27,** 189–205. ISSN: 1364-6613. https://www.sciencedirect.com/science/article/pii/S1364661322002984 (2023).
6. Antal, A. & Paulus, W. Transcranial alternating current stimulation (tACS). *Frontiers in Human Neuroscience* **7,** 54850. ISSN: 16625161 (June 2013).
7. Wu, L., Liu, T. & Wang, J. Improving the Effect of Transcranial Alternating Current Stimulation (tACS): A Systematic Review. *Frontiers in Human Neuroscience* **15,** 652393. ISSN: 16625161 (June 2021).
8. Elyamany, O., Leicht, G., Herrmann, C. S. & Mulert, C. Transcranial alternating current stimulation (tACS): from basic mechanisms towards first applications in psychiatry. *European Archives of Psychiatry and Clinical Neuroscience 2020 271:1* **271,** 135–156. ISSN: 1433-8491. https://link.springer.com/article/10.1007/s00406-020-01209-9 (Nov. 2020).
9. Polanía, R., Nitsche, M. A., Korman, C., Batsikadze, G. & Paulus, W. The Importance of Timing in Segregated Theta Phase-Coupling for Cognitive Performance. *Current Biology* **22,** 1314–1318. ISSN: 0960-9822. https://www.sciencedirect.com/science/article/pii/S096098221200574X (14 2012).
10. Strüber, D., Rach, S., Trautmann-Lengsfeld, S.-A. & et al. Antiphasic 40 Hz Oscillatory Current Stimulation Affects Bistable Motion Perception. *Brain Topography* **27,** 158–171. https://doi.org/10.1007/s10548-013-0294-x (2014).
11. Violante, I. R. *et al.* Externally induced frontoparietal synchronization modulates network dynamics and enhances working memory performance. *eLife* **6,** e22001 (2017).
12. Meng, Q. *et al.* Dual-site beta tACS over rIFG and M1 enhances response inhibition: A parallel multiple control and replication study. *International Journal of Clinical and Health Psychology* **23.** Cited by: 0; All Open Access, Gold Open Access, Green Open Access. https://www.sciencedirect.com/science/article/pii/S1697260023000479 (2023).
13. Tan, J. *et al.* The Effects of Dual-Site Beta tACS over the rIFG and preSMA on Response Inhibition in Young and Older Adults. *bioRxiv.* eprint: https://www.biorxiv.org/content/early/2023/06/01/2022.11.30.518460.full.pdf. https://www.biorxiv.org/content/early/2023/06/01/2022.11.30.518460 (2023).
14. Schwab, B. C., Misselhorn, J. & Engel, A. K. Modulation of large-scale cortical coupling by transcranial alternating current stimulation. *Brain Stimulation* **12,** 1187–1196. ISSN: 1935-861X (Sept. 2019).
15. Helfrich, R. F. *et al.* Selective Modulation of Interhemispheric Functional Connectivity by HD-tACS Shapes Perception. *PLOS Biology* **12,** 1–15. https://doi.org/10.1371/journal.pbio.1002031 (Dec. 2014).
16. Saturnino, G. B., Madsen, K. H., Siebner, H. R. & Thielscher, A. How to target inter-regional phase synchronization with dual-site Transcranial Alternating Current Stimulation. *NeuroImage* **163,** 68–80. ISSN: 1053-8119. https://www.sciencedirect.com/science/article/pii/S1053811917307723 (2017).
17. Minhas, P. *et al.* Electrodes for high-definition transcutaneous DC stimulation for applications in drug delivery and electrotherapy, including tDCS. *Journal of Neuroscience Methods* **190,**

188–197. ISSN: 0165-0270. https://www.sciencedirect.com/science/article/pii/S0165027010002669 (2010).
18. Dmochowski, J. P., Datta, A., Bikson, M., Su, Y. & Parra, L. C. Optimized multi-electrode stimulation increases focality and intensity at target. *Journal of Neural Engineering* **8,** 046011. https://doi.org/10.1088/1741-2560/8/4/046011 (2011).
19. Kuo, H.-I. *et al.* Comparing Cortical Plasticity Induced by Conventional and High-Definition 4×1 Ring tDCS: A Neurophysiological Study. *Brain Stimulation* **6,** 644–648. ISSN: 1935-861X. https://www.sciencedirect.com/science/article/pii/S1935861X12001830 (2013).
20. Ruffini, G., Fox, M. D., Ripolles, O., Miranda, P. C. & Pascual-Leone, A. Optimization of multifocal transcranial current stimulation for weighted cortical pattern targeting from realistic modeling of electric fields. *NeuroImage* **89,** 216–225. ISSN: 1053-8119. https://www.sciencedirect.com/science/article/pii/S1053811913012068 (2014).
21. Alekseichuk, I., Wischnewski, M. & Opitz, A. A minimum effective dose for (transcranial) alternating current stimulation. *Brain Stimulation* **15,** 1221–1222. ISSN: 1935-861X. https://www.sciencedirect.com/science/article/pii/S1935861X22001966 (2022).
22. Krause, M. R., Vieira, P. G., Csorba, B. A., Pilly, P. K. & Pack, C. C. Transcranial alternating current stimulation entrains single-neuron activity in the primate brain. *Proceedings of the National Academy of Sciences of the United States of America* **116,** 5747–5755. ISSN: 10916490. https://www.pnas.org/doi/abs/10.1073/pnas.1815958116 (Mar. 2019).
23. Johnson, L. *et al.* Dose-dependent effects of transcranial alternating current stimulation on spike timing in awake nonhuman primates. *Science Advances* **6.** ISSN: 23752548. https://www.science.org/doi/10.1126/sciadv.aaz2747 (Sept. 2020).
24. Schwab, B. C., König, P. & Engel, A. K. Spike-timing-dependent plasticity can account for connectivity aftereffects of dual-site transcranial alternating current stimulation. *NeuroImage* **237,** 118179. ISSN: 1053-8119 (Aug. 2021).
25. Zaehle, T., Rach, S. & Herrmann, C. S. Transcranial Alternating Current Stimulation Enhances Individual Alpha Activity in Human EEG. *PLOS ONE* **5,** 1–7. https://doi.org/10.1371/journal.pone.0013766 (Nov. 2010).
26. Fries, P. A mechanism for cognitive dynamics: neuronal communication through neuronal coherence. *Trends in Cognitive Sciences* **9,** 474–480. ISSN: 1364-6613. https://www.sciencedirect.com/science/article/pii/S1364661305002421 (2005).
27. Engel, A. K., Gerloff, C., Hilgetag, C. C. & Nolte, G. Intrinsic Coupling Modes: Multiscale Interactions in Ongoing Brain Activity. *Neuron* **80,** 867–886. ISSN: 0896-6273. https://www.sciencedirect.com/science/article/pii/S0896627313008696 (2013).
28. Alekseichuk, I. *et al.* Electric field dynamics in the brain during multi-electrode transcranial electric stimulation. *Nature Communications* **10,** 2573 (2019).
29. Zhang, L., Chen, L., Wang, Z., Liu, X. & Ming, D. Enhancing Motor Imagery Performance by Antiphasic 10 Hz Transcranial Alternating Current Stimulation. *IEEE Transactions on Neural Systems and Rehabilitation Engineering* **31.** Cited by: 1; All Open Access, Gold Open Access, 2747–2757. https://ieeexplore.ieee.org/document/10153632 (2023).
30. Heise, K. F., Monteiro, T. S., Leunissen, I. & et al. Distinct Online and Offline Effects of Alpha and Beta Transcranial Alternating Current Stimulation (tACS) on Continuous Bimanual Performance and Task-Set Switching. *Scientific Reports* **9,** 3144. https://doi.org/10.1038/s41598-019-39900-0 (2019).
31. Lang, E. W., Tomé, A. M., Keck, I. R., Górriz-Sáez, J. M. & Puntonet, C. G. Brain Connectivity Analysis: A Short Survey. *Computational Intelligence and Neuroscience* **2012,** 412512. https://doi.org/10.1155/2012/412512 (2012).
32. Soleimani, G., Kupliki, R., Bodurka, J., Paulus, M. P. & Ekhtiari, H. How structural and functional MRI can inform dual-site tACS parameters: A case study in a clinical population and its pragmatic implications. *Brain Stimulation* **15,** 337–351. ISSN: 1935-861X. https://www.sciencedirect.com/science/article/pii/S1935861X22000092 (2022).
33. Latrèche, C. *et al.* Using transcranial alternating current stimulation to enhance working memory skills in youths with 22q11.2 deletion syndrome: A randomized double-blind sham-controlled study. *Psychiatry Research* **335,** 115835. ISSN: 0165-1781. https://www.sciencedirect.com/science/article/pii/S0165178124001203 (2024).
34. Cohen, M. *Analyzing Neural Time Series Data: Theory and Practice* ISBN: 9780262019873. https://books.google.nl/books?id=jTSkAgAAQBAJ (MIT Press, 2014).

35. Cohen, M. X. *Complex Morlet wavelet convolution* Mike X Cohen. https://www.youtube.com/watch?v=uSslgfKmno0.
36. Cohen, M. X. *Averaging phase values* Mike X Cohen. https://www.youtube.com/watch?v=R1Pro555H6s.
37. Cohen, M. X. *Volume conduction and what to do about it* Mike X Cohen. https://www.youtube.com/watch?v=74qX6zG5Hn4.
38. Vinck, M., Oostenveld, R., van Wingerden, M., Battaglia, F. & Pennartz, C. M. An improved index of phase-synchronization for electrophysiological data in the presence of volume-conduction, noise and sample-size bias. *NeuroImage* **55,** 1548–1565. ISSN: 1053-8119. https://www.sciencedirect.com/science/article/pii/S1053811911000917 (2011).
39. Stam, C. J., Nolte, G. & Daffertshofer, A. Phase Lag Index: Assessment of Functional Connectivity from Multi-channel EEG and MEG with Diminished Bias from Common Sources. *Human Brain Mapping* **28,** 1178–1193. https://doi.org/10.1002/hbm.20346 (2007).
40. Nolte, G. *et al.* Identifying true brain interaction from EEG data using the imaginary part of coherency. *Clinical Neurophysiology* **115,** 2292–2307 (Oct. 2004).
41. Strüber, D., Rach, S., Neuling, T. & Herrmann, C. S. On the possible role of stimulation duration for after-effects of transcranial alternating current stimulation. *Frontiers in Cellular Neuroscience* **9.** Cited by: 69; All Open Access, Gold Open Access, Green Open Access. https://www.scopus.com/inward/record.uri?eid=2-s2.0-84940204715&doi=10.3389%2ffncel.2015.00311&partnerID=40&md5=1f35711d5df433d7f9d21489b3ace221 (2015).
42. Kohli, S. & Casson, A. J. Removal of Gross Artifacts of Transcranial Alternating Current Stimulation in Simultaneous EEG Monitoring. *Sensors (Basel, Switzerland)* **19,** 190. https://doi.org/10.3390/s19010190 (2019).
43. Nuwer, M. R. 10-10 electrode system for EEG recording. *Clinical Neurophysiology* **129,** 1103. ISSN: 1388-2457. https://www.sciencedirect.com/science/article/pii/S1388245718300907 (2018).
44. Timm, L. *NEW actiCAP and actiCHamp caps now with an improved and unified layout* https://www.brainproducts.com/newsdetails.php?set=219. Brain Products GmbH, July 2016.
45. Cohen, M. X. *Independent components analysis for removing artifacts* Mike X Cohen. https://www.youtube.com/watch?v=AKCK7DXa0gY.
46. Kaposzta, Z. *et al.* Fingerprints of Decreased Cognitive Performance on Fractal Connectivity Dynamics in Healthy Aging. *GeroScience* **46,** 713–736. https://doi.org/10.1007/s11357-023-01022-x (2024).
47. Filippi, M., Spinelli, E. G., Cividini, C. & Agosta, F. Resting State Dynamic Functional Connectivity in Neurodegenerative Conditions: A Review of Magnetic Resonance Imaging Findings. *Frontiers in Neuroscience* **13,** 657. https://doi.org/10.3389/fnins.2019.00657 (2019).
48. Chiang, S. *et al.* Time-Dependence of Graph Theory Metrics in Functional Connectivity Analysis (I7.001). *Neurology* **86,** I7.001. eprint: https://www.neurology.org/doi/pdf/10.1212/WNL.86.16_supplement.I7.001. https://www.neurology.org/doi/abs/10.1212/WNL.86.16_supplement.I7.001 (2016).
49. Fraschini, M. *et al.* The effect of epoch length on estimated EEG functional connectivity and brain network organisation. *Journal of Neural Engineering* **13,** 036015. eprint: https://doi.org/10.1088/1741-2560/13/3/036015. https://doi.org/10.1088/1741-2560/13/3/036015 (June 2016).
50. Chu, C. J. *et al.* Emergence of Stable Functional Networks in Long-Term Human Electroencephalography. *Journal of Neuroscience* **32,** 2703–2713. https://doi.org/10.1523/JNEUROSCI.5669-11.2012 (Feb. 2012).
51. Tort, A. B. L., Komorowski, R., Eichenbaum, H. & Kopell, N. Measuring Phase-Amplitude Coupling Between Neuronal Oscillations of Different Frequencies. *Journal of Neurophysiology* **104.** PMID: 20463205, 1195–1210. eprint: https://doi.org/10.1152/jn.00106.2010. https://doi.org/10.1152/jn.00106.2010 (2010).
52. Wischnewski, M. *et al.* NMDA Receptor-Mediated Motor Cortex Plasticity After 20 Hz Transcranial Alternating Current Stimulation. *Cerebral Cortex* **29,** 2924–2931. ISSN: 1047-3211. eprint: https://academic.oup.com/cercor/article-pdf/29/7/2924/28907126/bhy160.pdf. https://doi.org/10.1093/cercor/bhy160 (July 2018).
53. Berger, A., Pixa, N. H., Steinberg, F. & Doppelmayr, M. Brain oscillatory and hemodynamic activity in a bimanual coordination task following transcranial alternating current stimulation (TACS): A combined EEG-fNIRS study. *Frontiers in Behavioral Neuroscience* **12,** 335494. ISSN: 16625153 (Apr. 2018).
54. Canolty, R. T. *et al.* High gamma power is phase-locked to theta oscillations in human neocortex. *Science* **313,** 1626–1628 (2006).

55. Fiene, M. *et al.* Phase-specific manipulation of rhythmic brain activity by transcranial alternating current stimulation. *Brain Stimulation* **13,** 1254–1262. ISSN: 1935-861X (Sept. 2020).
56. Hülsemann, M. J., Naumann, E. & Rasch, B. Quantification of Phase-Amplitude Coupling in Neuronal Oscillations: Comparison of Phase-Locking Value, Mean Vector Length, Modulation Index, and Generalized-Linear-Modeling-Cross-Frequency-Coupling. *Frontiers in Neuroscience* **13,** 573 (2019).
57. S. S. Shapiro & M. B. Wilk. An analysis of variance for normality (complete samples). *Biometrika* **52** (1965).
58. Bufacchi, R. J., Magri, C., Novembre, G. & Iannetti, G. D. Local Spatial Analysis: An Easy-to-Use Adaptive Spatial EEG Filter. *Journal of Neurophysiology* **125,** 509–521. `https://doi.org/10.1152/jn.00560.2019` (2021).